N62-14463

GENERAL ELECTRIC

MISSILE AND SPACE DIVISION

TECHNICAL INFORMATION SERIES

Title Page

AUTHOR	SUBJECT CLASSIFICATION	No.
R. H. Edsall	Aerodynamic Flow Fields	62SD186
		DATE 31 July 1962

TITLE: Calculation of Flow Fields about Blunt Bodies of Revolution Traveling at Escape Velocity*

ABSTRACT: The method of Gravalos for calculating the inviscid flow about blunt supersonic bodies has been applied to the case of a hemisphere-cylinder at escape velocity. Numerical results are presented for the flow variables throughout the shock layer, both near the nose and downstream along the cylinder. The results are compared with data from six flow fields at lower velocities in order to illustrate the effects peculiar to escape-velocity re-entry. The body pressures and shock shapes computed by this method agree well with available experimental data at Mach numbers from 3 to 10, and are correlated fairly well by cylindrical blast-wave parameters.

G.E. CLASS	REPRODUCIBLE COPY FILED AT	No. PAGES
1	MSD Library - Doc. Library Unit VF-STC King of Prussia, Penna.	
GOV. CLASS. Uncl.		

* This work was supported under NASA Contract NAS 5-302.

By cutting out this rectangle and folding on the center line, the above information can be fitted into a standard card file.

INFORMATION PREPARED FOR

TESTS MADE BY Robert H. Edsall
Engineer, Aerodynamics Operation

COUNTERSIGNED Herbert H. Ridyard
Supervisory Engineer, Aerodynamics Operation

J S Arnaiz
Manager, Aerodynamics Operation

DIVISION Missile and Space LOCATION 3198 Chestnut Street, Philadelphia 4, Pa.

ACKNOWLEDGEMENTS

The flow field analysis used to obtain the results in this paper was developed by F. G. Gravalos, with the collaboration of I. H. Edelfelt, H. W. Emmons, and V. A. Langelo. J. W. Friedhofer programmed the equations for the IBM 704 digital computer. The numerical results were obtained with the assistance of Mrs. M. E. O'Brien and Mrs. C. T. Hill, whose help is gratefully acknowledged.

TABLE OF CONTENTS

Section		Page
1.	INTRODUCTION	7
2.	ANALYSIS	11
3.	NUMERICAL RESULTS	25
4.	CONCLUDING REMARKS	39
5.	REFERENCES	43
6.	NOTATION	49
	TABLE 1	52
	FIGURES	53

1. INTRODUCTION

The development of high-speed re-entry vehicles has stimulated a number of studies, both theoretical (References 1-36) and experimental (References 37-50) pertaining to the aerodynamics of high-speed flows. Work has concentrated on flow about bodies of revolution; blunt bodies are of importance since excessive heat transfer to the nose must be avoided. Re-entry at hypervelocities is characterized by formation of a bow shock envelope about the body, with hot dissociated and ionized flow in a shock layer surrounding the vehicle. At the very least, the chemical reactions serve to drop the temperatures far below values predicted on the basis of ideal gas calculations. The real-gas effects are important in communication problems, where the electron density is of paramount concern, and real-gas effects may alter significantly the aerodynamic force and moment coefficients of the body.

The difficulty in simulating high enthalpy flows experimentally has given increased impetus to analytical efforts at predicting the flow characteristics for hypersonic re-entry. Such approximate theories as Newtonian (Reference 13), constant-density (Reference 13), small-disturbance (References 4, 32), and blast-wave (Reference 21), though very useful for some purposes, are inadequate to solve the complete flow field about a blunt body. The analytical difficulties associated with the compressible flow equations are so great that closed-form exact solutions for an entire class of blunt-body flows appear to be unattainable. Hence much attention has been directed toward development

of numerical procedures suitable for calculating the flow for a given body shape and given free-stream conditions, with a view toward use of correlations and similarity laws to extend the usefulness of the results.

Methods of solving the blunt body problem may be divided into two classes: (1) the direct problem (References 1,10, 11, 28), in which the body shape is specified and the shock wave location and the flow field are to be determined; and (2) the inverse problem (References 9,29, 33), in which the shock shape is specified and the flow field and the body shape are to be determined. Most of the calculations which have been reported have been for flow of ideal gases, though several of the methods are adaptable to real dissociating gases.

Inverse blunt-body solutions are obtained by forward integration of the governing equations from the shock toward the streamline which defines the body. In obtaining inverse solutions by the methods cited above, the bow shock wave is often chosen so as to give an approximation to a desired body shape. The question then arises of how closely the calculated body should agree with the body of interest, or, to restate the question, how accurately the calculated flow field represents the true flow about the body of interest. A deficiency of the inverse methods arises from the insensitivity of shock wave location to local changes in body contour. It is clear that the flow conditions near the surface of an irregular body, and in particular the surface pressures, would be extremely difficult to obtain by specifying the shock shape and performing

forward integrations. Solutions of the direct blunt-body problem are preferred for most applications, since the body shape is usually the specified boundary condition for the flow equations, while the shock wave location is not known a priori. The direct methods generally encounter some difficulty in calculating the shock wave location, but are satisfactory in the neighborhood of the specified body.

A rather complete review of the various blunt-body methods has been given by Hayes and Probstein, and therefore the details of the methods, and their merits and limitations, need not be discussed here. However, since Reference 13 does not consider the method (Reference 11) used to obtain the numerical results in this report, and since many of the details of the procedures used have not been published previously, it is appropriate to describe the analysis in some detail.

2. ANALYSIS

In this section we shall describe the method used to obtain the present flow field results at escape velocity. This solution of the direct blunt-body problem was derived by Gravalos and co-workers (References 10,11). It is applicable to the inviscid supersonic flow about a blunt body of revolution at zero angle of attack. The method may be used for both ideal gas flow (Reference 10) and equilibrium real gas flow (Reference 11). The approach used is well-suited to numerical computations by high speed digital computers; the equations have been programmed for the IBM 704 computer. The procedure which is used has the advantage of flexibility in treating a variety of blunt-body configurations over a wide range of Mach numbers. For a given Mach number - altitude condition, the transonic region is calculated by a streamtube method. Results of this calculation can supply initial data for calculating the supersonic region of flow over different afterbodies. Calculations for various cases agree well with available experimental data; some comparisons with data for flow about hemisphere-cylinders will be discussed in Section 3.

The governing inviscid steady-state flow equations for conservation of mass, momentum, and energy are taken to be

$$\nabla \cdot (\rho \bar{V}) = 0 \tag{1}$$

$$\frac{D\bar{V}}{Dt} = (\bar{V} \cdot \nabla)\, \bar{V} = -\frac{1}{\rho}\, \nabla p \tag{2}$$

$$\frac{Ds}{Dt} = \bar{V} \cdot \nabla s = 0 \tag{3}$$

The analysis, which proceeds from these basic equations, can be conveniently divided into four separate topics: (1) representation of the thermodynamic

properties of equilibrium gases; (2) change in the flow conditions across an oblique shock wave; (3) flow in the subsonic and transonic region; (4) flow in the supersonic region. A detailed outline of the four facets of the analysis and computational procedure will now be given.

Representation of Gas Properties

The flow field analysis described in Reference 11 is applicable to gases which are in chemical equilibrium and also to ideal gases as a special case. The thermodynamic properties are accounted for by use of a quantity γ^* defined by

$$\gamma^* \equiv \left(\frac{\partial \ell n p}{\partial \ell n \rho}\right)_s \equiv \frac{\rho}{p}\left(\frac{\partial p}{\partial \rho}\right)_s \equiv \frac{c^2 \rho}{p} \tag{4}$$

which is analogous to the specific heat ratio γ for ideal gases. Tabular values of γ^* (p, s), presumed to be available, are approximated in the piece-wise linear form

$$\gamma^* = \frac{a(s)}{p} + b(s). \tag{5}$$

The analytical usefulness of this representation is twofold. Taking $p = p(\rho, s)$, the total derivative $dp/d\rho$ along a streamline is identically equal to $(\partial p/\partial \rho)_s$. Then from Equations (4) and (5) there follows, upon integration, the isentropic relation between pressure and density along a streamline:

$$\frac{a + bp}{\rho^b} = K. \tag{6}$$

The definition of γ^* given in Equations (4) and (5) also permits immediate integration of the equation of motion along a streamline,

$$V\frac{dV}{ds} + \frac{1}{\rho}\frac{dp}{ds} = 0, \tag{7}$$

to give an "energy equation" which relates velocity, pressure, and density:

$$\frac{V^2}{2} + \frac{1}{b-1}\frac{a+bp}{\rho} = C. \tag{8}$$

The Mach number is given by

$$M = \frac{V}{\sqrt{\frac{a+bp}{\rho}}}. \tag{9}$$

The values of a, b are required for a sufficient number and range of entropies to permit linear interpolations in the flow field calculations to be performed. If more than one set of a, b is required to fit the gas properties over the range of pressures to be encountered in the flow field calculations, as is the case for air, proper adjustment of K and C at the "pressure breaks" must be made.

The values of the isentropic functions a and b for air in chemical equilibrium have been calculated for temperatures in the range 300° K - $15,000^{\circ}$ K and pressures in the range 10^{-4} - 10^{2} atmospheres. Acoustic velocity data of the National Bureau of Standards (Reference 51) were cross-plotted to obtain γ^* as a function of pressure and entropy for temperatures of 300° K - 3000° K. The thermodynamic data for Logan and Treanor (Reference 55) were used as the source of γ^* for temperatures in the range 3000° K - $10,000^{\circ}$K. In order to obtain flow field results at escape velocity, for which stagnation temperatures nearing $15,000^{\circ}$ K occur, additional data for acoustic velocity were required. The only available source appears to be the tables of Hochstim (Reference 54), which were obtained by numerical differentiations of the basic high-temperature data of Hilsenrath and Beckett (Reference 52). Although the quantity γ^* derived

in this way is less accurate than the original data because of the numerical operations, a comparison with the results of Logan and Treanor in the region of overlap has shown agreement to within 1% or better. Hochstim presented interpolated values of γ^* along isentropes, at given temperatures. From these results it was simple to obtain the functional relationship required for this study by replacing temperature by pressure as one of the independent variables. The tables were then plotted in the form γ^* vs. 1/p for constant s/R. Over the six decades of pressure considered, the curves behaved quite erratically because of excitation of the various degrees of freedom of the molecules. Hence in order to obtain 1% or better fit to the data, the constants a, b given by Equation (5) were obtained for each of twelve pressure ranges. The straight lines were forced to meet at the bounds of the pressure ranges, so that consistent data are provided for the flow field calculations along isentropes. The process of finding a and b is shown in Figure 2 for the particular value s/R = 50.

The computer programs used to obtain the escape-velocity flow field utilize several tables of thermodynamic data in addition to the "a and b tables" described above. The compressibility factor Z and the modified specific heat ratio $\overline{\gamma} \equiv h/e$ are required in the shock computations. These have been entered in the form

$$Z(\rho, T) = A_o + A_1 T + \ldots + A_7 T^7 \tag{10}$$

$$\overline{\gamma}\ (\rho,\ T) = B_o + B_1 T + \ldots + B_7 T^7, \tag{11}$$

with the coefficients A_i and B_i determined by least-squares curve fits to the data

of Hilsenrath and Beckett (Reference 52). The A_i and B_i were obtained for each of the 41 density ratios in Reference 52, and in order to represent the data very accurately the curve fits were made over several limited ranges of temperature. Minor adjustments of A_o and B_o were made at the temperature breaks to give a continuous approximation to the data. In addition, quadratic and cubic curve fits of the low-temperature data in Reference 51 were obtained.

The programs also require look-up tables for $s(\rho, p)$ and $Z(\rho, s)$. These were obtained from cross-plots of the data in References 51 and 55.

The thermodynamic data described above are for air in chemical equilibrium. It should be emphasized, however, that the Gravalos flow field method is applicable to any equilibrium gas which is sufficiently well-behaved to permit the use of the piece-wise linearization described above, and for which the required thermodynamic data are available. For example, a study is now being made of the blunt-body flow of a gas representative of the atmosphere of Venus.

Shock Calculation

The calculation of flow in the transonic and supersonic regions requires that shock data corresponding to given free-stream conditions and local shock angle be available. This section will describe the shock analysis, using the notation indicated in Figure 3. For the present analysis and results it has been assumed that the shock wave is a mathematical discontinuity across which the laws for conservation of mass, momentum, and energy must be satisfied. The conservation laws for mass $\mathcal{M}$, normal momentum $\mathcal{N}$, tangential momentum $\mathcal{I}$,

and energy $\mathcal{E}$ may be written in the form

$$\mathcal{M} \equiv \rho_\infty V_\infty \sin\sigma = \rho_2 V_2 \sin(\sigma - \theta) \tag{12}$$

$$\mathcal{N} \equiv p_\infty + \rho_\infty V_\infty^2 \sin^2\sigma = p_2 + \rho_2 V_2^2 \sin^2(\sigma - \theta) \tag{13}$$

$$\mathcal{T} \equiv V_\infty \cos\sigma = V_2 \cos(\sigma - \theta) \tag{14}$$

$$\mathcal{E} \equiv \frac{\overline{\gamma}_\infty}{\overline{\gamma}_\infty - 1}\frac{p_\infty}{\rho_\infty} + \frac{V_\infty^2}{2} = \frac{\overline{\gamma}_2}{\overline{\gamma}_2 - 1}\frac{p_2}{\rho_2} + \frac{V_2^2}{2}. \tag{15}$$

In the energy equation (15) the quantity $\frac{\overline{\gamma}}{\overline{\gamma} - 1}\, p/\rho$ is used instead of enthalpy h.

The equation of state for an ideal dissociating gas is assumed to apply:

$$p_2 = Z_2 \rho_2 R T_2. \tag{16}$$

The flow field techniques described in this report may be used for either ideal gases ($Z = 1$, $\overline{\gamma} = C_p/C_v$) or real gases in chemical equilibrium. In the latter case the compressibility factor Z and the modified specific heat ratio $\overline{\gamma}$ are assumed to be known functions of density and temperature.

Equations (12) - (16) constitute a set of five equations in the five unknown quantities ρ_2, p_2, T_2, V_2, θ. The method of solution which has been used was developed by Langelo (Reference 18). It is not greatly different from that of more recent investigations (e. g. References 14, 17) but it will be briefly outlined here for the sake of completeness. Equations (12) - (14) are substituted into Equation (15) to eliminate the variables V_2, p_2, θ; there results a quadratic equation for the density ρ_2:

$$\left(\mathcal{E} - \tfrac{1}{2}\mathcal{T}^2\right)\rho_2^2 - \frac{\overline{\gamma}_2}{\overline{\gamma}_2 - 1}\mathcal{N}\rho_2 + \left(\frac{\overline{\gamma}_2}{\overline{\gamma}_2 - 1} - \frac{1}{2}\right)\mathcal{M}^2 = 0 \tag{17}$$

Using a first approximation for $\bar{\gamma}_2$, which may be taken as $\bar{\gamma}_\infty$, Equation (17) yields the density ρ_2. The larger root is the correct one for well-behaved real gases such as air (Reference 12). Equations (12) and (13) may be combined to give the pressure p_2:

$$p_2 = \mathcal{K} - \frac{\mathcal{M}^2}{\rho_2}. \tag{18}$$

A new approximation to the temperature is determined from Equation (16), using an appropriate loop for the product $Z_2 T_2$. An improved value of $\bar{\gamma}_2$ is then obtained from the least-squares curve fits described earlier. The process is repeated, starting from Equation (17), until the temperature is constant to four significant figures. The values of T_2, ρ_2, and p_2 on the final iteration are used, together with V_2 and θ obtained from Equations (12) and (14):

$$V_2 = \sqrt{\frac{\mathcal{M}^2}{\rho_2^2} + \mathcal{J}^2}, \tag{19}$$

$$\theta = \sigma - \cos^{-1} \frac{\mathcal{J}}{V_2}. \tag{20}$$

Transonic Region

The flow over a blunt-nosed supersonic body is characterized by the occurrence of a detached shock wave and regions of subsonic and supersonic flow separated by a sonic line (or surface). Solution of the subsonic flow region is of considerable interest in itself, and is essential for the calculation of the supersonic flow since the location of the sonic line is not known beforehand. The mathematical complexity caused by the mixed character of the flow and the

unknown location of the shock wave has been described by Hayes and Probstein (Reference 13), among others. The iterative method of solution used in the present calculations, which was developed by Gravalos et al. (References 10, 11), will be discussed in this section. This "transonic method" yields the flow variables throughout the inviscid subsonic and transonic regions, including the body pressure distribution, shock shape, and sonic line location, for the case of zero angle of attack.

The notation to be followed is shown in Figure 4. The body is specified by a series of points (x_i, r_i), together with body slopes and curvatures at these points. (Length dimensions are referred to the nose diameter, or some other reference length, while the flow variables are treated in dimensional form, using engineering units.) Initial estimates of the static pressures on the body at (x_i, r_i) are chosen. Lacking better information, the modified Newtonian values

$$p = p_t \sin^2\theta + p_\infty \cos^2\theta \tag{21}$$

may be used. An initial estimate of the shock shape is also required, in the form of a fifth order polynomial in r^2:

$$x_s = a_0 + a_1 r_s^2 + \ldots a_5 r_s^{10}. \tag{22}$$

The governing equations are solved in the streamline-normal coordinate system depicted in Figure 4. If we define the value of the stream function by $\psi_\infty = \pi r^2 \rho_\infty V_\infty$, the mass flow in the streamtube bounded by the m^{th} and $m-1^{th}$ streamlines is

$$\psi_m - \psi_{m-1} = \pi \Delta n(r_m \rho_m V_m + r_{m-1} \rho_{m-1} V_{m-1}), \tag{23}$$

where

$$r_m = r_{m-1} + \frac{\Delta n}{2} (\cos\theta_m + \cos\theta_{m-1}). \tag{24}$$

The equation for conservation of momentum normal to the streamline,

$$\frac{\partial p}{\partial n} = \frac{\rho V^2}{R}, \tag{25}$$

is treated in the finite-difference form

$$p_m - p_{m-1} = \frac{\Delta n}{2} \left(\frac{\rho_m V_m^2}{R_m} + \frac{\rho_{m-1} V_{m-1}^2}{R_{m-1}} \right). \tag{26}$$

We also have the isentropic relation for a real gas from Equation (6),

$$\frac{a + bp_m}{\rho_m b} = K_m \tag{27}$$

The parameter K_m is obtained from the oblique-shock data for the given streamline. In general K_m changes discontinuously at points where the streamline being considered crosses pressure breaks in the γ^* fits, as described in detail in Reference 11. The equation of motion along the streamline is Equation (8),

$$\frac{V_m^2}{2} + \frac{1}{b-1} \frac{a + bp_m}{\rho_m} = C_m. \tag{28}$$

The parameter C_m, like K_m, is obtainable from shock data and changes at points where the streamline crosses pressure breaks. Finally, we should note the equation for Mach number,

$$M_m = \frac{V_m}{\sqrt{\frac{a+bp_m}{\rho_m}}}. \tag{29}$$

The step-by-step procedure used in the transonic flow calculation will now be described. From the assumed body pressures and the known normal-shock entropy, Equation (27) is solved for density at the body points. The velocity and Mach number at the body points are then found from Equations (28) and (29) respectively.

The calculation of each streamline other than the body streamline must be performed a number of times, using successive approximations to the radius of curvature R of the streamline. Consider, for instance, the calculation of the m^{th} streamline away from the body. It is specified in terms of the free-stream mass flow $\Delta\psi$ in the streamtube bounded by it and the $m-1^{th}$ streamline. A set of $\Delta\psi$ values, which define the starting radial coordinates of the streamlines to be computed, is required for the transonic calculations. Consider the mesh point which is at the intersection of the m^{th} streamline with the n^{th} normal. From the continuity Equation (23), an estimate of the streamtube width Δn shown in Figure 4 may be obtained from

$$\Delta n = \frac{\Delta\psi}{2\pi\rho_{m-1}V_{m-1}r_{m-1}} \quad . \tag{30}$$

From Equation (26), an estimate of the pressure at this mesh point is

$$p_m = p_{m-1} + \Delta n \frac{\rho_{m-1}V_{m-1}^2}{R_{m-1}} \tag{31}$$

where, for the first calculation of the m^{th} streamline, we take $R_m = R_{m-1}$. To improve the accuracy of the calculation of p_m by Equation (26), improved values of ρ_m, V_m, and Δn are obtained using Equations (27), (28), and (23). A convergence criterion specifies the accuracy desired in determining the

streamline location. Then the succeeding points n+1, n+2, ... along the streamline are calculated in an identical manner. After the entire streamline has been found, it is necessary to repeat the calculation at each mesh point, using improved values of R_m. These are obtained by parabolic fit of the coordinates of the points n-1, n, n+1 found during the previous calculation of this streamline. A convergence criterion for the streamline curvatures could be used, but, since experience has shown that two calculations of each streamline are sufficient to give good results, this criterion is used instead. Each of the streamlines outward from the body is calculated in the above manner.

As each streamline at the n^{th} normal is obtained, a continuity check is made. This is done by comparing the radial coordinate r_m of the m^{th} streamline with the radial coordinate $(r_s)_m$ which corresponds to the mass flow between this streamline and the body. As may be seen from Figure 4, $r_m > (r_s)_m$ for points within the shock layer. When some streamline c is reached at which the condition $r_c = (r_s)_c$ is met to within a specified accuracy, the mass flow across normal n is equal to the mass flow through the shock. This defines a "continuity point" (x_c, r_c) which terminates normal n. The continuity points for all normals, taken together, provide essential information for subsequent adjustments of the assumed shock shape and body pressure distribution. In general there is a difference between the pressure at the continuity point as determined using Equation (26) and the pressure obtained from the oblique shock wave solution, using the assumed shock shape. This difference reflects a need to adjust the pressure level in this region of the shock layer. Some fraction of the pressure difference, say 10%, is added algebraically to the body pressure

at normal n. Graphical smoothing of the new body pressures determined in this way is usually required before another iteration is attempted. A least-squares curve fit to the continuity points is often used for the shock shape on the next iteration, though on occasion the shock shape may be held fixed, and only the body pressures adjusted. The process of converging a transonic solution is often difficult, and it has been found that a considerable amount of experience and judgment are necessary to effect a rapid convergence. Usually from five to twenty attempts are required before the continuity points fall on the assumed shock wave and the continuity point pressures agree with the oblique-shock pressures to within 1%. Efforts to automate the procedure, avoiding the loss of calendar time between iterations, have not yet been completely successful.

Converged solutions which have been obtained during the four years of use of the transonic flow field method at GE-MSVD include some 40 real-air cases at various velocity-altitude conditions, 7 ideal cases (γ = 1.4, 1.67), and 2 cases corresponding to certain shock tunnel conditions. The majority of these solutions have been for spherical forebodies, though a few have been for Apollo-type blunt bodies. The method works well in the hypersonic and moderate supersonic speed ranges, but for free-stream Mach numbers below about 3 there are difficulties in the numerical integration which appear to be attributable to the increased shock layer thickness. The choice of altitude is limited only by the assumption of continuum flow and use of the equation of state discussed earlier.

The transonic method described above gives shock layer results in both the subsonic flow and a portion of the supersonic flow. The calculations can be carried without difficulty to body stations at which the flow is supersonic. Initial data along a "transonic normal" are thus available for the calculation of the supersonic flow over the remainder of the body, using the method described below.

Supersonic Region

The supersonic flow calculation proceeds from initial data supplied by the transonic calculations just described. It is done by the usual method of characteristics, e.g., Reference 13, pp. 253-257, taking pressure and flow angle as the dependent variables. Flow properties are calculated at the mesh points of left-running characteristics ℓ^+ and right-running characteristics ℓ^-. The equations governing changes in p and θ are, respectively,

$$\frac{d\theta}{d\ell^+} + \frac{\sqrt{M^2-1}}{\rho V^2}\frac{dp}{d\ell^+} + \frac{\sin\theta}{Mr} = 0, \tag{32}$$

$$\frac{d\theta}{d\ell^-} - \frac{\sqrt{M^2-1}}{\rho V^2}\frac{dp}{d\ell^-} - \frac{\sin\theta}{Mr} = 0. \tag{33}$$

The computer program which was devised calculates along right-running characteristics from the input line or the shock to the body. The calculation of data at a field point "C" (see Figure 1) from data at two points "A", "B", which must be on a non-characteristic line, will now be described. Equations (32), (33) are used in finite-difference form. An initial estimate of the location of point C, i.e. (x_C, r_C), is obtained as the intersection of Mach lines through A

and B at angles $\theta_A - \mu_A$, $\theta_B + \mu_B$ from the horizontal, respectively. From this information $\Delta\ell^+$, $\Delta\ell^-$ and r_C are obtained. Initial estimates of ρ_C, V_C, and M_C are also obtained, from the corresponding values at points A and B. Equations (32) and (33) then yield first iterates for p_C and θ_C. The entropy s_C is found from s_A and s_B by a linear interpolation. Improved values of ρ_C, V_C, and M_C, corresponding to p_C and s_C, are then found from Equations (6), (8), and (9). Moreover, a better approximation to the location x_C, r_C is found by using average values M_{AC}, M_{BC} for the two Mach lines. The calculation of pressure and flow angle from Equations (32) and (33) is repeated using average values of the parameters until appropriate convergence criteria have been met.

The above calculation applies for finding conditions at mesh points which do not lie on the shock or the body. A shock point S is located at the intersection of the extended shock wave from a known shock point and the left-running characteristic from a known field point. The pressure and the flow angle at S are found by simultaneous solution of Equation (32) and the oblique shock relations. Successive improvements to the coefficients in Equation (32) are made in a manner similar to that described above for field points, until appropriate convergence criteria have been met. A body point B is located at the intersection of a right-running characteristic with the given body contour. Since the flow angle and entropy are known, the pressure follows immediately from Equation (33), and the remaining flow variables are then easily obtained.

3. NUMERICAL RESULTS

Since the main purpose of the study reported here was to investigate the dynamic and thermodynamic effects peculiar to blunt-body flow at extremely high speeds, it was decided to limit the calculations to a single body configuration. Many earlier theoretical and experimental studies of flow at supersonic speeds have been made for the case of a hemisphere-cylinder, which appears to be a fundamental blunt-body shape of interest in re-entry applications, so this configuration was selected for the present investigation.

The free-stream conditions used in this study were chosen to be 36,000 ft/sec velocity and 100,000 ft. altitude. From point-mass trajectory calculations (Ref. 20), it appears that such conditions might be reached upon return from lunar orbit at a re-entry angle of approximately 25^{o} or greater, or upon return from interplanetary ventures at smaller re-entry angles. One reason for selecting an altitude below approximately 200,000 ft. was the belief that thermodynamic equilibrium within the shock layer is more likely to obtain at relatively low altitudes. For purposes of comparison, pressure and shock shape data from six other hemisphere-cylinder flow fields will be presented also. See Table I for the assumed flight conditions. The 1959 ARDC model of the earth's atmosphere (Ref. 56) was used for the free-stream properties corresponding to the specified altitudes. In the discussion and figures, the seven flow fields often will be cited by their respective Mach numbers, for the sake of convenience, but it should be emphasized that for hypersonic real-gas flows the velocity is of more fundamental importance.

Earlier theoretical work dealing with supersonic flow about hemisphere-cylinders will be briefly reviewed, in order to set the framework for the new results to be presented here. Feldman (Ref. 6) calculated a real-gas flow field by the method of characteristics, starting from transonic data calculated by the method of Belotserkovskii using $\gamma = 1.2$. Detailed results of the shock layer structure were given, showing the existence of a large low-density high-entropy region near the cylinder. Van Hise (Ref. 35) obtained ideal-gas flow fields for hemisphere-cylinders using a sonic cone starting solution. He gave results for body pressure distributions and shock shapes at several Mach numbers. Vaglio-Laurin and Trella (Ref. 30) calculated flow of equilibrium air and ideal gas about a hemisphere-cylinder at Mach numbers ranging from 7.7 to 22 using the inverse blunt body method of Vaglio-Laurin and Ferri (Ref. 29) to obtain the subsonic and transonic region. Seiff and Whiting (Ref. 24) derived a method of determining flow in the subsonic and supersonic regions using the continuity equation together with an assumed shock shape, and compared shock layer profiles with unpublished results obtained by Gravalos' method (Ref. 11). Available experimental data for supersonic flow over hemisphere-cylinders, which are limited to body pressures and shock shapes, are summarized and compared with new flow field results below.

In addition to the work dealing with hemisphere-cylinders there have been many theoretical investigations of the supersonic flow about a sphere, and there are many pressure and shock shape data for spheres and spherically-blunted cones which are pertinent to the present investigation. In the discussion

to follow, some of these data will be compared with flow field results. However, a review of the mass of information available for spheres will not be attempted in this paper.

Oblique Shock Wave

The conditions immediately following an oblique shock wave have been calculated for shock angles of $90^{\circ} > \sigma > \sin^{-1} 1/M_{\infty}$ at increments of 0.5 degree by the method described in Section 2. Flight speeds of 28,000 ft/sec, 32,000 ft/sec and 36,000 ft/sec at 100,000 ft. altitude were assumed. The two lower-velocity solutions were obtained in order to assess the real-gas effects which occur with increasing velocity. The results for density, compressibility, temperature and pressure are shown in Figures 5 and 6.

There are several interesting features of the high-velocity shocks which will be discussed here. At shock angles for which $Z \approx 1.2$ the density and temperature curves have inflections associated with oxygen dissociation. Results at lower velocities have shown a characteristic increase of density as the shock strength is increased. We see from Figure 5, however, that for escape velocity shocks the density reaches a maximum at approximately $\sigma = 50^{\circ}$ and falls to a somewhat smaller value at the normal shock. This same effect can be seen from the normal-shock curves of Huber (Ref. 17) as Mach number is varied, corresponding to shock obliquity. This phenomenon is also seen in the extensive calculations of Hochstim (Ref. 14) in which the free-stream temperature 273.16° K was assumed. In fact, his results show that the density overshoot occurs even more strongly at high altitudes, as a result of the increased dissociation and

ionization which accompany rarefaction. It is noteworthy that the Mach number behind the shock (not shown) is nearly unity at maximum flow deflection, in agreement with results at lower velocities. Finally, it should be mentioned that the sonic condition occurs at a larger shock angle as the velocity is increased.

The fact that oblique-shock conditions are obtained from normal shock results by considering only the flow component at right angles to the shock wave is well-known. Reversing the logic, the plotted oblique shock data in Figures 5 and 6 could be converted to a wide range of normal shocks at less extreme velocities. Indeed, the data at 28, 000 ft/sec and 32, 000 ft/sec could have been obtained from the 36, 000 ft/sec results quite easily.

The oblique shock results at V_∞ = 36, 000 ft/sec have been used as input data for the transonic and supersonic flow field calculations described below.

Spherical Nose

The transonic flow field method described in Section 2 has been used to calculate the subsonic* and transonic region of flow about a hemispherical forebody at a velocity of 36, 000 ft/sec and an altitude of 100, 000 ft. The

*It should be mentioned that, because of inaccuracies associated with the streamline-normal mesh, the transonic flow program does not provide precise definition of the flow in the immediate vicinity of the stagnation point. A subsonic flow field program which calculates the flow details in this region by a relaxation method using boundary data from the transonic flow program was developed, but it has not been used in this study.

supersonic region of flow was then obtained by the method of characteristics. The thermodynamic tables and oblique-shock data described earlier were used as input to the calculations. Before the numerical results are presented, several details of the calculations will be discussed.

For the present calculation twelve normals were originated at the body, at the stations θ: 84° (5°) 29°. Four streamlines crossed the first normal before it reached the shock, while 31 streamlines crossed the twelfth normal. Figure 7 shows the locations of the normals and several of the streamlines from the converged solution.

It has been found from experience that the iteration procedure, consisting of successive approximations to the body pressure distribution and the shock shape, converges rapidly for high-velocity flow fields because of the thinness of the shock layer. There is relatively little opportunity for accumulation of errors in the integration across the shock layer, and also the difference between the oblique-shock pressure and the continuity pressure at a given normal is closely associated with the error in body pressure at that normal. For the present calculation the first estimates at body pressure and shock shape were made by scaling results from a converged transonic flow field at 25,400 ft/sec. Only four iterations were required for satisfactory convergence. This was considered to have been obtained when the pressures at the continuity points were within 1% of the corresponding oblique-shock pressures and the locations of the continuity points agreed with the final assumed shock shape. Some approximation such as modified Newtonian theory could have furnished the first iterate for pressure, but more iterations would have been required.

The supersonic characteristics calculation was begun using data from the eighth normal of the converged transonic solution. The variables p, ρ, V, M, θ were plotted, and eighteen points (x, r) were selected at which to read the input data.* The computer calculation gave results in the supersonic region of the nose and downstream along the cylinder.

The pressure distribution over most of the hemisphere has been found to be significantly lower than predicted by the modified Newtonian theory expression

$$C_p/C_{p_{max}} = \sin^2\theta. \tag{34}$$

The comparison is shown in Figure 8. Also shown are the converged pressure distributions, computed by Gravalos' method, for several other real-gas flow fields at the indicated velocities. The flow field results deviate immediately from the modified Newtonian prediction, though the sparseness of mesh points near the stagnation point (see earlier footnote) introduces some error in this vicinity. At a station one-half of the distance around the sphere there appears to be a definite trend away from Newtonian theory as the free-stream velocity increases, in agreement with calculations of Vaglio-Laurin and Trella (Ref. 30) over a smaller velocity range. For the escape-velocity case modified

*This number of input points had been found to be satisfactory from the standpoint of accuracy and running time by extensive numerical work with the program for the case of a slender 10^o spherically-blunted cone.

Newtonian theory overpredicts the pressure coefficient by as much as 25% at body stations of approximately 30^{o}. The shock tunnel data of Nagamatsu, Geiger, and Shear (Ref. 47) at a Mach number of ten, shown in Figure 8 for comparison, tend to substantiate the flow field results. The data are from runs at stagnation temperatures of 1400^{o}K to 5300^{o}K, but the nozzle flow may not have been in chemical equilibrium at the higher stagnation temperatures. Experimental data for sphere pressures at real-gas flow conditions nearer to those assumed in the flow field calculations are not available.

In order to assess the relative importance of real-gas effects upon the sphere pressure distribution, and to provide a comparison of flow field results with experimental data, several ideal gas flow fields have been computed by Gravalos' method. The body pressures are presented in Figure 9. The flow field results and the data of Baer (Ref. 37), Machell and O'Bryant (Ref. 46), and Crawford and McCauley (Ref. 39) appear to be in agreement that Newtonian theory somewhat overestimates the pressure coefficient on much of the sphere. The same qualitative effect is found in the inverse blunt-body calculations by Van Dyke and Gordon (Ref. 34) and Vaglio-Laurin and Trella (Ref. 30). On the other hand, the data of Oliver (Ref. 48) and Julius (Ref. 40) agree very well with the Newtonian prediction.

It is not clear from the flow field results shown in Figure 9 whether the continuing effect of velocity changes upon pressure coefficient noted for the real-gas cases occurs for ideal gases also. This could probably be determined by calculating ideal-gas flow fields at higher Mach numbers by Gravalos' method.

The results of Van Dyke and Gordon and unpublished calculations by Ridyard (Ref. 23) using Van Dyke's method definitely indicate that the ideal-gas pressure coefficient is virtually independent of Mach number for Mach numbers of 15 or greater.

From the above considerations it is concluded that the velocity trend of $C_p/C_{p_{max}}$ shown in Figure 8 is a real-gas effect attributable to molecular dissociation. The principle of Mach number independence derived for ideal gases (Ref. 13, pp. 24-26) is not valid for real air flow fields at these velocities, at least with regard to surface pressure coefficient. This is associated with the fact that the normal-shock density ratio continues to vary as the Mach number becomes very large.

Figure 10 summarizes a number of flow field results for the pressure coefficient ratio at the shoulder ($\theta = 0^{o}$). The ratio has been found to be approximately 0.04 for a free-stream Mach number of about 15. For lower Mach numbers it is significantly less, and there is a slight downward trend at higher Mach numbers. Newtonian theory, of course, predicts a pressure coefficient of zero at the shoulder. Figure 8 shows that a Prandtl-Meyer expansion continuation of the Newtonian curve, starting at the location where the two methods have the same pressure gradients and using an average γ of 1.2, overestimates the shoulder pressure coefficient by a factor of two for the escape velocity case.

The shock-wave locations about the spherical nose are shown in Figure 11 for four of the flow fields. The shock waves become progressively

nearer the body as the free-stream Mach number is increased.* Figure 11 also shows the sonic lines for the four flow fields. The location of the sonic point at the body changes little with free-stream velocity. For Mach numbers of 3.5 (ideal gas), 10 (real gas), and 35.885 (real gas) the sonic line at the body points upstream in the "usual" manner. However, for Mach 5.0 (real gas) it initially points slightly downstream of the normal to the body. This may be due to the lowered effective γ, which is approximately 1.36 for this case. There is a significant movement of the oblique-shock sonic point toward the body axis as the free-stream velocity is increased. As the free-stream velocity is varied, the extent of the subsonic flow region is strongly affected by both the change in shock detachment distance and the change in sonic line location.

The computational method for the transonic flow region yields data at the intersection points of a streamline-normal grid. The results in the supersonic flow region are at characteristic mesh points. In order to present the data in a useful and illustrative form search-interpolation programs were written which give constant-property lines in the flow field. These routines search down each streamline (or right-running characteristic) until the mesh points which bracket a desired property are found. The coordinates x, r are then obtained by a linear interpolation. Figures 12a-f, which were obtained by plotting these coordinates, show the contours of constant Mach number, density,

temperature, pressure, and velocity in the shock layer about the spherical nose. The density curves in the stagnation region behave oddly because of the dissociation phenomena, as discussed earlier in connection with the oblique shock conditions. Downstream of the stagnation region, the density increases from the body to the shock. The temperature falls from the stagnation value of 24,400°R to approximately 14,000°R at the tangency point with the cylinder. Its variation from body to shock is 25% or less. As discussed earlier, the pressure distribution on the sphere surface is somewhat less than predicted by modified Newtonian theory, except at flow angles of less than 20°. Pressure is nearly constant across the shock layer in the stagnation region, but downstream it increases from body to shock in approximate proportion to the density variations.

Cylindrical Afterbody

The real-gas supersonic flow field at Mach 35.885 was calculated by the method of characteristics. As described earlier, eighteen input points were obtained from plotted results of the transonic program. The computed body pressures from the tangency point x/d = 0.5 to x/d = 15 are shown in Figure 13. Available experimental data are also shown, along with pressure distributions from six additional flow fields. The cylinder pressure data of Baer (Ref. 37) at Mach numbers of 3, 4.03, 5.06 and 8.10 at a stagnation temperature of 100° F and Reynolds number per inch of 4×10^5 offer striking confirmation of the flow field calculations at Mach numbers of 3.5, 5.0 and 8.0. These results

*Shock shapes as determined from a number of real-gas flow fields for spheres have been correlated as a simple function of normal-shock density ratio by R. J. Berman (Ref. 2). His results have been submitted for publication elsewhere.

and earlier experimental investigations (Ref. 42) at Mach numbers of 1 to 4 show the presence of overexpansion near the shoulder. Unfortunately no accurate data for pressures on a spherically-blunted cylinder are available for Mach numbers above about eight. Hotshot data (Ref. 38) at Mach numbers from 11 to 18 and stagnation temperatures of approximately 6000^{o}K have too large a scatter to permit meaningful comparison with the flow field curves. The high pressure level of the escape-velocity case and its rather gradual decay toward the free-stream value are noteworthy. Five nose diameters downstream the static pressure is more than ten times the free-stream value.

An attempted correlation of experimental and theoretical results for pressures along a spherically-blunted cylinder using the cylindrical blast-wave parameter (Ref. 21) is shown in Figure 14. The correlation shown is limited to axial stations from two to fifteen nose diameters from the stagnation point, regardless of free-stream Mach number, in order to illustrate the range of applicability of the blast-wave theory. At high Mach numbers the equation given by the second-order blast-wave analogy (Ref. 21) for $\gamma = 1.4$,

$$\frac{p}{p_\infty} = 0.067 \frac{M_\infty^2 \sqrt{C_D}}{x/d} + 0.44, \tag{35}$$

overpredicts the pressures near the nose by about 75% but further downstream it gives good results. At intermediate Mach numbers the agreement is generally satisfactory for x/d from two to fifteen. At low Mach numbers the blast theory predicts a larger over-expansion effect than actually occurs. Of course, the assumptions inherent in the blast-wave approximation make it inapplicable to flows at low Mach numbers.

The characteristics calculations reported by Van Hise (Ref. 35) for an ideal gas with $\gamma = 1.4$ agree well with the correlation shown in Figure 14 when the blast parameter is 0.01 or greater. When it is less than 0.01 his results follow the second-order blast-wave prediction rather than the present ideal and real gas flow field pressures. This is probably due to the fact that at high Mach numbers Van Hise includes data only far downstream of the nose in accordance with the range of validity of the blast wave theory. Casaccio (Ref. 3) has presented a hemisphere-cylinder pressure distribution at $M_\infty = 20$, from a characteristics calculation for an ideal gas with $\gamma = 1.4$, using the inverse blunt-body method in Ref. 29 for a starting solution. His results fall much further below the blast wave prediction than do the present flow field results in Figure 13. Feldman's calculations (Ref. 6) by the method of characteristics for the case of a hemisphere-cylinder at a velocity of 17,500 ft/sec and an altitude of 60,000 ft. were carried to an axial distance x/d = 50. His results indicate that the second-order blast-wave theory overpredicts the cylinder pressure by 30% at x/d = 10 but is more accurate for both larger and smaller x/d. The present flow field results at $V_\infty = 21,000$ ft/sec, by way of contrast, show excellent agreement with the blast-wave theory curve near x/d = 10 (Figure 14). In Feldman's calculations such agreement was obtained only for x/d of about 20 or greater. Whether this discrepancy between the two analytical results is attributable to the difference in free-stream conditions, or whether it arises from the use of different methods of calculation, is not known.

Shock shapes obtained by theory and experiments are compared in Figure 15. The data of Baer at Mach 3 and Mach 4 bracket the flow field result for Mach 3.5 as would be expected. Data at Mach 3.55 (Love, Ref. 45), Mach 5 (Baer), and Mach 9.85 (Seiff and Whiting, Ref. 49) agree well with flow field results at Mach numbers of 3.5, 5, and 10, respectively, although the tests were conducted at ideal-gas conditions whereas the calculations for Mach 5 and 10 were for equilibrium air. It should be noted that the shock-wave location for the 36,000 ft/sec flow field is somewhat nearer the cylinder than that for the 21,000 ft/sec case, indicating that the Mach number independence with regard to shock shape is being approached but has not been reached.

A correlation of the theory and data according to the second-order blast-wave analogy is shown in Figure 16. The suggested equation (Ref. 21),

$$\frac{r/d}{M_\infty \sqrt{C_D}} = 0.795 \left(\frac{x/d}{M_\infty^2 \sqrt{C_D}} \right)^{\frac{1}{2}} \left(1 + 3.15 \frac{x/d}{M_\infty^2 \sqrt{C_D}} \right)^{\frac{1}{2}}, \quad (36)$$

predicts Mach number independence for shock shape, the last factor in Equation (36) being unity at high Mach numbers. Equation (36) underpredicts the radial shock coordinate by about 5%, on the average. For the escape-velocity case the agreement is excellent, but this is considered to be merely coincidental. An effective value for γ for the flow field, according to the criterion suggested in Ref. 30, would be approximately 1.25, but the corresponding blast-wave equation does not give as good a fit to the shock shape.

Details of the flow over the cylinder are shown by constant-lines plots in Figures 17 a-f. The constancy of pressure (at given axial station) across half the shock layer thickness is a notable feature of the flow. The high temperature and low density near the cylinder's surface are due to the fact that the gas in this region has passed through the strong portion of the bow shock wave. The shock-layer profiles of pressure, temperature, density and velocity at given axial station appear to be in qualitative agreement with Feldman's results (Ref. 6).

4. CONCLUDING REMARKS

The escape-velocity flow field results which have been presented in this paper are valid for an altitude of 100, 000 ft. Although exact scaling of the results to other altitudes is not possible for air in chemical equilibrium, experience in calculating many hypersonic flow fields has shown that the following approximate rules are sufficiently accurate for most engineering purposes. To scale density (or pressure), multiply the present results by the ratio of ambient densities (or pressures) at the two altitudes. Temperature, velocity, Mach number and flow angle should be left unchanged. These rules apply only to dissociated hypersonic flow. For ideal gas flow fields at a given Mach number the variables ρ, p, T, V scale exactly by the ratios of the corresponding free-stream properties, while M and θ remain unchanged.

A major limitation on the validity of the results which have been presented is the neglect of fluid viscosity. Boundary layer effects may be expected to alter significantly the flow near the surface of the cylinder. Whereas the inviscid flow field predicts a region of high velocity, high temperature, low density dissociated gas there, it is well-known that the absence of slip at the wall, together with wall cooling, results in a large velocity gradient and a boundary layer of relatively cool high-density flow. However, since methods for treating real-gas boundary layer development in such a high-speed external flow are rather complex and, on the whole, lack substantiation, no numerical corrections to the inviscid flow field results have been attempted. Generally speaking, the boundary layer on the cylinder at 100, 000 ft. altitude is probably thin and turbulent, and its effects

upon the body pressure distribution, the shock shape, and most of the flow field should be minor.

A second important assumption, that of chemical equilibrium, is probably valid in the low-velocity region near the spherical nose because of the relatively large residence times and the high temperatures and pressures there. Downstream, however, particularly in the low-density region adjacent to the cylinder, deviations from equilibrium may occur. Large deviations would be expected for flow fields at altitudes of approximately 200,000 ft. or higher, but the effect may be minor at the altitude of 100,000 ft. for which the present results were obtained.

Estimates of the equilibrium-flow electron densities in the ionized layer about the hemisphere-cylinder may be readily made using the escape-velocity flow field results for temperature and density. Tables of electron mole fractions for equilibrium air at high temperatures have been prepared by Hilsenrath and Beckett (Ref. 53). From these data, the electron density at the stagnation point is found to be approximately 7×10^{17} cm^{-3}. At ten nose diameters downstream, the value near the cylinder's surface is 6×10^{13} cm^{-3}. By way of contrast, the corresponding values for the flow field at 21,000 ft/sec velocity and 100,000 ft. altitude are 3×10^{15} cm^{-3} and 7×10^{12} cm^{-3}. The greatly increased electron densities associated with re-entry at escape velocity may be of considerable importance in communication and detection problems.

The numerical results which have been presented were calculated using computer programs for the supersonic flow about a smooth blunt body of revolution at zero angle of attack. Brief mention should be made of several compatible programs which have been developed subsequently at GE-MSVD. One program calculates the Prandtl-Meyer expansion at a sharp convex corner of a blunt body, and the flow downstream of it. Another obtains the secondary shock wave resulting from a sharp concave corner, together with the flow downstream of it. Still a third calculates the flow field at arbitrarily small angle of attack by a perturbation method. The problem of calculating flow fields which include intersecting bow and secondary shock waves is now being programmed for the IBM 7090 computer. Finally, it should be mentioned that the flow field analyses and programs are applicable to both two-dimensional and axially-symmetric flows. For clarity and conciseness this paper has been limited to axially-symmetric cases.

5. REFERENCES

1. Belotserkovskii, O. M., "Flow with a Detached Shock Wave about a Symmetrical Profile", Jour. Appl. Math. and Mech. (PMM), Vol. 22, No. 2, 1958, pp. 279-296.

2. Berman, R. J., Private communication.

3. Casaccio, A., "Theoretical Pressure Distribution on a Hemisphere-Cylinder Combination", Jour. Aero. Sci. (Readers' Forum), Vol. 26, No. 1, January 1959, pp. 63-64.

4. Cheng, H. K., et al., "Boundary Layer Displacement and Leading Edge Bluntness Effects in High-Temperature Hypersonic Flow", Journal Aero/Space Sci., Vol. 28, No. 5, May 1961, pp. 353-382.

5. Dorodnicyn, A. A., "A Contribution to the Solution of Mixed Problems of Transonic Aerodynamics", in Advances in Aeronautical Sciences, Vol. 2, Pergamon Press, N. Y., 1959, pp. 832-844.

6. Feldman, S., "Numerical Comparison Between Exact and Approximate Theories of Hypersonic Inviscid Flow Past Slender Blunt-Nosed Bodies", ARS Journal, Vol. 30, No. 5, May 1960, pp. 463-468.

7. Ferri, A., "A Review of Some Recent Developments in Hypersonic Flow", in Advances in Aeronautical Sciences, Vol. 2, Pergamon Press, N. Y., 1959, pp. 723-770.

8. Fuller, F. B., "Numerical Solutions for Supersonic Flow of an Ideal Gas about Blunt Two-Dimensional Bodies", NASA TN D-791, July 1961.

9. Garabedian, P. R., and Lieberstein, H. M., "On the Numerical Calculation of Detached Bow Shock Waves in Hypersonic Flow", IAS Journal, Vol. 25, No. 2, February 1958, pp. 109-118.

REFERENCES (Cont'd.)

10. Gravalos, F. G., "Supersonic Flow About a Blunt Body of Revolution", in Advances in Astronautical Sciences, Vol. 2 (Proc. 4th Annual Meeting, Amer. Astron. Soc., December 1957). Plenum Press, N. Y., 1958.

11. Gravalos, F. G., Edelfelt, I. H., and Emmons, H. W., "The Supersonic Flow about a Blunt Body of Revolution for Gases at Chemical Equilibrium", 9th Annual Congress of International Astronautical Federation, Amsterdam, August 1958.

12. Hammit, A. G., "Further Comments on 'Mach Line Determination for Air in Dissociation Equilibrium'", Jour. Aero/Space Sci., Readers' Forum, Vol. 28, No. 8, August 1961, pp. 659-660.

13. Hayes, W. D., and Probstein, R. F., Hypersonic Flow Theory, Academic Press, N. Y., 1959.

14. Hochstim, A. R., "Gas Properties Behind Shocks at Hypersonic Velocities: I. Normal Shocks in Air", Convair ZPH-002, January 1957.

15. Holt, M., and Hoffman, G. H., "Calculation of Hypersonic Flow Past Spheres and Ellipsoids", IAS-ARS Preprint No. 61-209-1903, June 1961.

16. Holt, M., "Direct Calculation of Pressure Distribution on Blunt Hypersonic Nose Shapes with Sharp Corners", Jour. Aero/Space Sci., Vol. 28, No. 11, November 1961, pp. 872-876.

17. Huber, P. W., "Tables and Graphs of Normal-Shock Parameters at Hypersonic Mach Numbers and Selected Altitudes", NACA TN 4352, September 1958.

REFERENCES (Cont'd.)

18. Langelo, V. A., "Flow Across a Shock Front", General Electric Company Report TIS R56SD135, August 1956.

19. Li, T. Y., and Geiger, R. E., "Stagnation Point of a Blunt Body in Hypersonic Flight", Jour. Aero/Space Sci., Vol. 24, No. 1, January 1957, p. 25.

20. Lovelace, U. M., "Charts Depicting Kinematic and Heating Parameters for a Ballistic Reentry at Speeds of 26,000 to 45,000 Feet per Second", NASA TN D-968, October 1961.

21. Lukasiewicz, J., "Blast-Hypersonic Flow Analogy Theory and Application", ARS Preprint No. 2169-61, October 1961.

22. Ridyard, H. W., "Comparison of the Ionized Shock Layer about Two and Three Dimensional Blunt Shapes at Hypersonic Speeds", General Electric Company Report TIS R60SD327, February 1960.

23. Ridyard, H. W., Private communication.

24. Seiff, A., and Whiting, E. E., "Calculation of Flow Fields from Bow Wave Profiles for the Downstream Region of Blunt Nosed Circular Cylinders in Axial Hypersonic Flight", NASA TN D-1147, November 1961.

25. Stamm, S. L., "A Representation of the Thermodynamic Properties of Air in Chemical Equilibrium for Calculating Isentropic Processes", General Electric Company Report TIS R59SD415, August 1959.

26. Traugott, S. C., "An Approximate Solution of the Direct Supersonic Blunt-Body Problem for Arbitrary Axisymmetric Shapes", Jour. Aero/Space Sci., Vol. 27, No. 5, May 1960, pp. 361-370.

REFERENCES (Cont'd.)

27. Traugott, S. C., "Some Features of Supersonic and Hypersonic Flow about Blunted Cones", Jour. Aero/Space Sci., Vol. 29. No. 4, April 1962, pp. 389-399.

28. Uchida, S., and Yasuhara, M., "The Rotational Field Behind a Curved Shock Wave Calculated by the Method of Flux Analysis", IAS Journal, Vol. 23, No. 9, September 1956, pp. 830-845.

29. Vaglio-Laurin, R., and Ferri, A., "Theoretical Investigation of the Flow Field about Blunt Nosed Bodies in Supersonic Flight", Jour. Aero/Space Sci., Vol. 25, No. 12, December 1958, pp. 761-770.

30. Vaglio-Laurin, R., and Trella, M., "A Study of Flow Fields about Some Typical Blunt-Nosed Slender Bodies", Polytechnic Institute of Brooklyn, Report No. 623, December 1960.

31. Vaglio-Laurin, R., "On the PLK Method and the Supersonic Blunt-Body Problem", J. Aero/Space Sci., Vol. 29, No. 2, February 1962, pp. 185-206.

32. Van Dyke, M. D., "A Study of Hypersonic Small-Disturbance Theory", NACA Report 1194, 1954.

33. Van Dyke, M. D., "The Supersonic Blunt-Body Problem - Review and Extension", Jour. Aero/Space Sci., Vol. 25, No. 8, August 1958, pp. 485-496.

34. Van Dyke, M. D., and Gordon, H., "Supersonic Flow Past a Family of Blunt Axisymmetric Bodies", NASA Technical Report R-1, 1959.

35. Van Hise, V., "Analytic Study of Induced Pressure on Long Bodies of Revolution with Varying Nose Bluntness at Hypersonic Speeds", NASA Technical Report R-78, 1960.

REFERENCES (Cont'd.)

36. Yakura, J. K., "A Theory of Entropy Layers and Nose Bluntness in Hypersonic Flow", ARS Preprint No. 1983-61, August 1961.

37. Baer, A. L., "Pressure Distributions on a Hemisphere Cylinder at Supersonic and Hypersonic Mach Numbers", AEDC TN 61-96, August 1961.

38. Boison, J. C., "Experimental Investigation of the Hemisphere-Cylinder at Hypervelocities in Air", AEDC TR 58-20, November 1958.

39. Crawford, D. H., and McCauley, W. D., "Investigation of the Laminar Heat-Transfer Characteristics of a Hemisphere-Cylinder in the Langley 11-Inch Hypersonic Tunnel at a Mach Number of 6.8", NACA TN 3706, July 1956.

40. Julius, J. D., "Experimental Pressure Distributions over Blunt Two- and Three Dimensional Bodies Having Similar Cross-Sections at a Mach Number of 4.95", NASA TND-157, September 1959.

41. Kaegi, E. M. et al, "The Capabilities of the Shock Tunnel in the Study of the Aerodynamics of Atmospheric Entry", ARS Preprint 1554-60, December 1960.

42. Katz, J. R., "Pressure and Wave Drag Coefficients for Hemispheres, Hemisphere-Cones and Hemisphere-Ogives", NAVORD Report 5849, March 1958.

43. Lees, L., and Kubota, T., "Inviscid Hypersonic Flow over Blunt-Nosed Slender Bodies", IAS Journal, Vol. 24, No. 3, March 1957, pp. 195-202.

44. Lewis, C. H., "Pressure Distribution and Shock Shape over Blunted Slender Cones at Mach Numbers from 16 to 19", AEDC TN 61-81, August 1961.

REFERENCES (Cont'd.)

45. Love, E. S., "A Reexamination of the Use of Simple Concepts for Predicting the Shape and Location of Detached Shock Waves", NACA TN 4170, December 1957.

46. Machell, R. M., and O'Bryant, W. T., "An Experimental Investigation of the Flow over Blunt-Nosed Cones at a Mach Number of 5.8", CALCIT Hypersonic Research Project Memo No. 32, June 1956.

47. Nagamatsu, H. T., Geiger, R. E., and Sheer, R. E., Jr., "Real Gas Effects in Flow over Blunt Bodies at Hypersonic Speeds", J. Aero/Space Sci., Vol. 27, No. 4, April 1960, pp. 241-251.

48. Oliver, R. E., "An Experimental Investigation of Flow about Simple Blunt Bodies at a Nominal Mach Number of 5.8", J. Aero. Sci., Vol. 23, No. 2, February 1956, pp. 177-179.

49. Seiff, A., and Whiting, E. E., "A Correlation of the Bow-Wave Profiles of Blunt Bodies", NASA TN D-1148, February 1962.

50. Stine, H. A., and Wanlass, K., "Theoretical and Experimental Investigation of Aerodynamic Heating and Isothermal Heat-Transfer Parameters on a Hemispherical Nose with Laminar Boundary Layer at Supersonic Mach Numbers", NACA TN 3344, December 1954.

51. Hilsenrath, J. et al., Tables of Thermal Functions of Gases, NBS Circular 564, November 1955.

52. Hilsenrath, J. and Beckett, C. W., "Tables of Thermodynamic Properties of Argon-Free Air to 15,000^{o}K, AEDC TN 56-12, September 1956.

53. Hilsenrath, J. and Beckett, C. W., addendum to Ref. 52, unpublished.

REFERENCES (Cont'd.)

54. Hochstim, A. R., "Gas Properties Behind Shocks at Hypersonic Velocities: III. Tables of Thermodynamic Properties of Air", Convair ZPh-004, August 1958.

55. Logan, J. G. and Treanor, C. E., "Tables of Thermodynamic Properties of Air from 3000°K to 10,000°K at Intervals of 100°K", Cornell Aero. Lab. Report No. BE-1007-A-3, January 1957.

56. Minzner, R. A., Champion, K. S. W. and Pond, H. L., "The ARDC Model Atmosphere, 1959", Air Force Surveys in Geophysics, No. 115, AFCRC-TR-59-267, August 1959.

6. NOTATION

a, b	isentropic functions in Equation (5)
$a_0 - a_5$	coefficients in Equation (22)
c	equilibrium speed of sound
d	nose diameter
e	internal energy
h	enthalpy; also, altitude
p	static pressure
r	radial coordinate
s	entropy; also, distance along streamline
x	axial coordinate

NOTATION (Cont'd.)

$A_0 - A_7$	coefficients in Equation (10)
$B_0 - B_7$	coefficients in Equation (11)
C	isentropic function in Equation (8)
C_D	nose drag coefficient
C_p	pressure coefficient $(p - p_\infty) / 1/2\, \rho_\infty\, V_\infty^2$; also, specific heat at constant pressure
C_v	specific heat at constant volume
D/Dt	$\partial/\partial t + \bar{V} \cdot \nabla$
K	isentropic function in Equation (6)
M	Mach number
R	specific gas constant for undissociated mixture; also, local radius of curvature of streamline
S	shock point
T	temperature
V	velocity
Z	compressibility factor, $p = Z\rho RT$
ℓ^+	coordinate along left-running characteristic
ℓ^-	coordinate along right-running characteristic
$\mathcal{E}$	free-stream energy, Equation (15)
$\mathcal{M}$	free-stream mass flow normal to shock, Equation (12)
$\mathcal{N}$	free-stream momentum flow normal to shock, Equation (13)
$\mathcal{J}$	free-stream momentum flow tangential to shock, Equation (14)
γ	C_p/C_v

NOTATION (Cont'd.)

$\bar{\gamma}$	h/e
γ^*	isentropic function defined by Equation (4)
ψ	stream function
ρ	density
σ	shock angle measured from horizontal
θ	flow angle measured from horizontal
Δn	incremental distance out transonic normal
$\Delta \psi$	mass flow through streamtube

Subscripts

c	continuity point
m	number of streamline
s	refers to shock wave
t	stagnation
C	field point in supersonic region
max	stagnation
2	conditions after oblique shock
∞	free-stream

TABLE I

ASSUMED FREE STREAM CONDITIONS AND

CALCULATED STAGNATION PRESSURE AND DRAG COEFFICIENTS

M_∞	V_∞ (ft/sec)	h (ft)	p_∞ (lb/ft^2)	$C_{p_{max}}$	C_D
3.5		(ideal gas)		1.778	.99
5.0	5080	25,000	786.3	1.815	.96
8.0		(ideal gas)		1.826	.88
10.0	9681	40,000	393.1	1.871	.95
18.0		(ideal gas)		1.837	.878
20.933	21,000	100,000	23.085	1.921	.925
35.885	36,000	100,000	23.085	1.926	.880

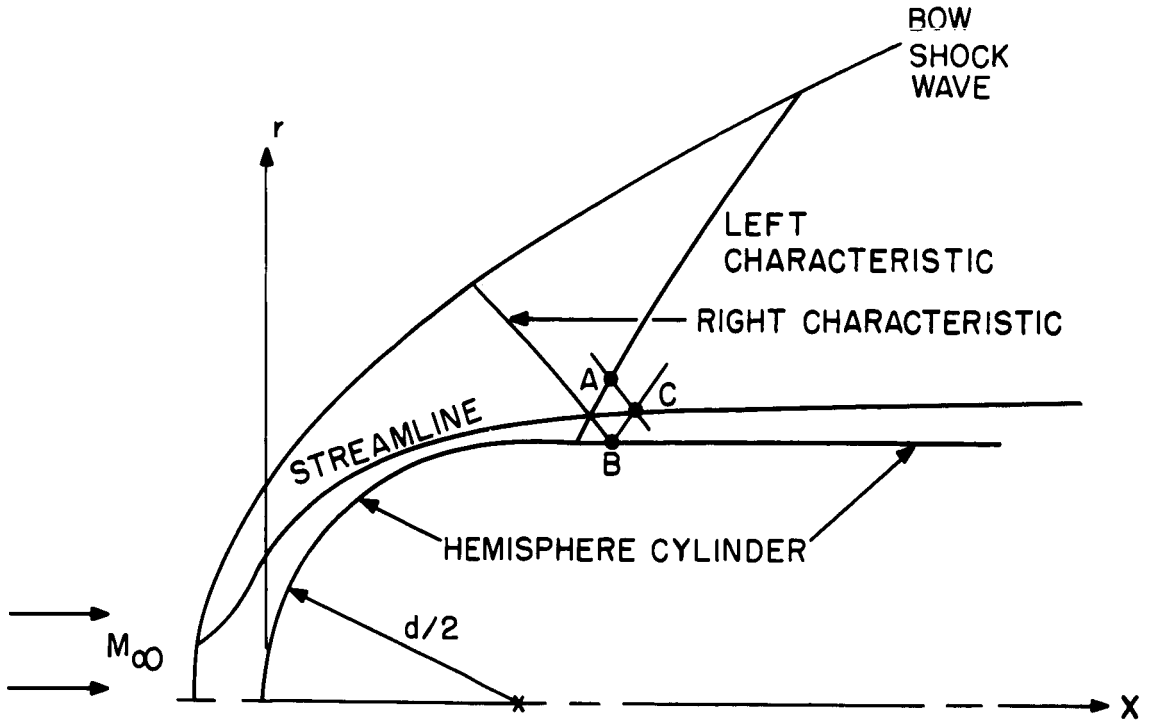


Figure 1. Sketch of Supersonic Flow about a Blunt Body

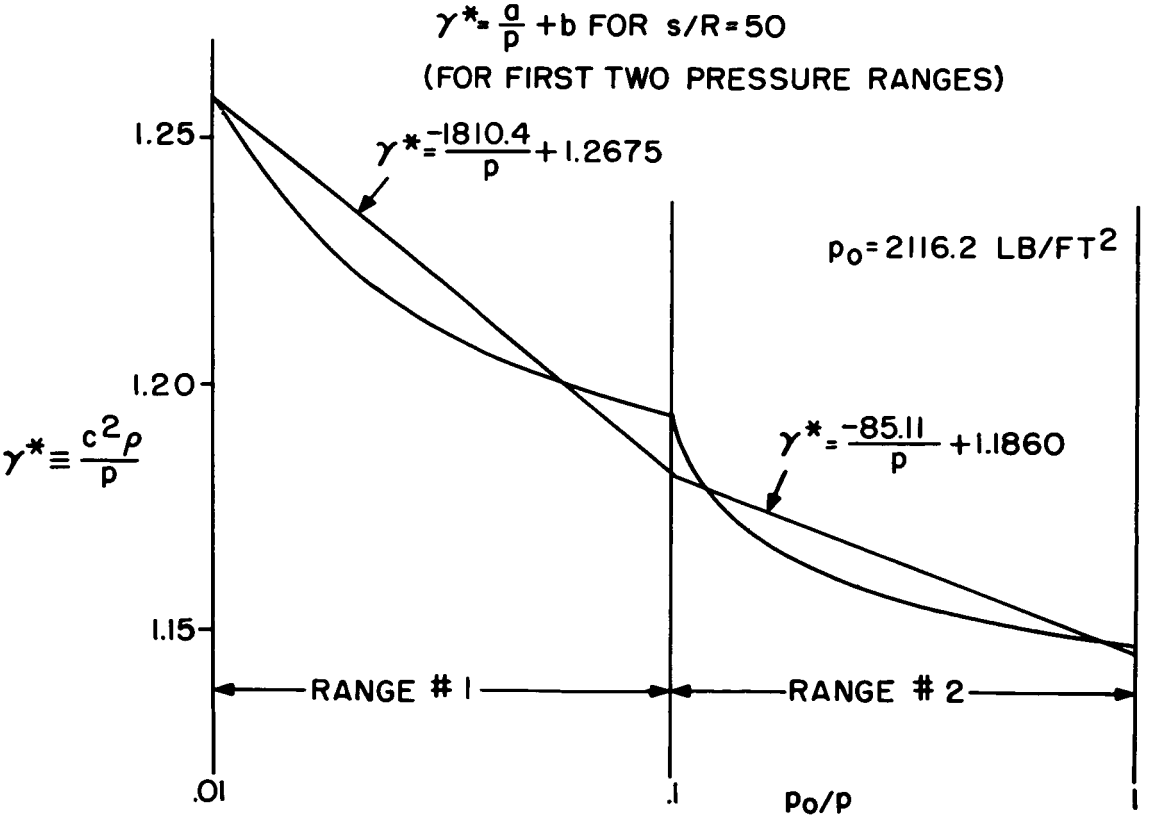


Figure 2. Representation of Air Properties

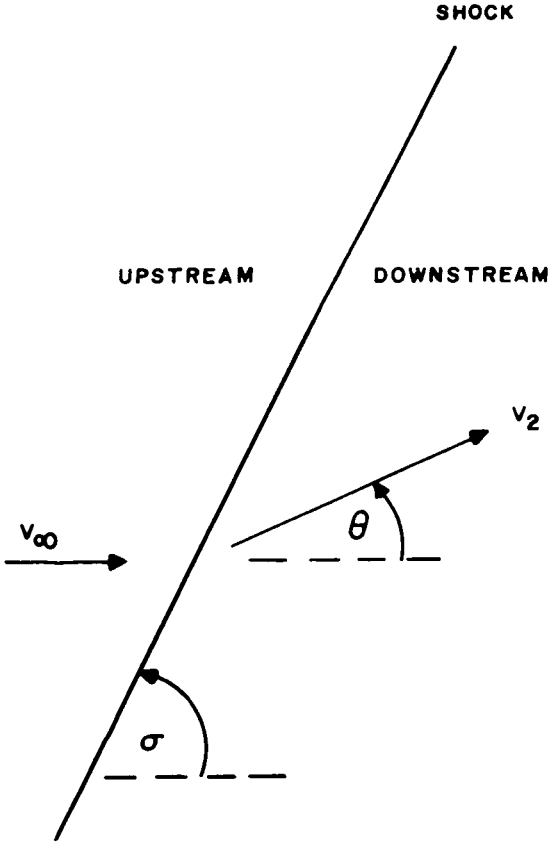


Figure 3. Oblique Shock Notation

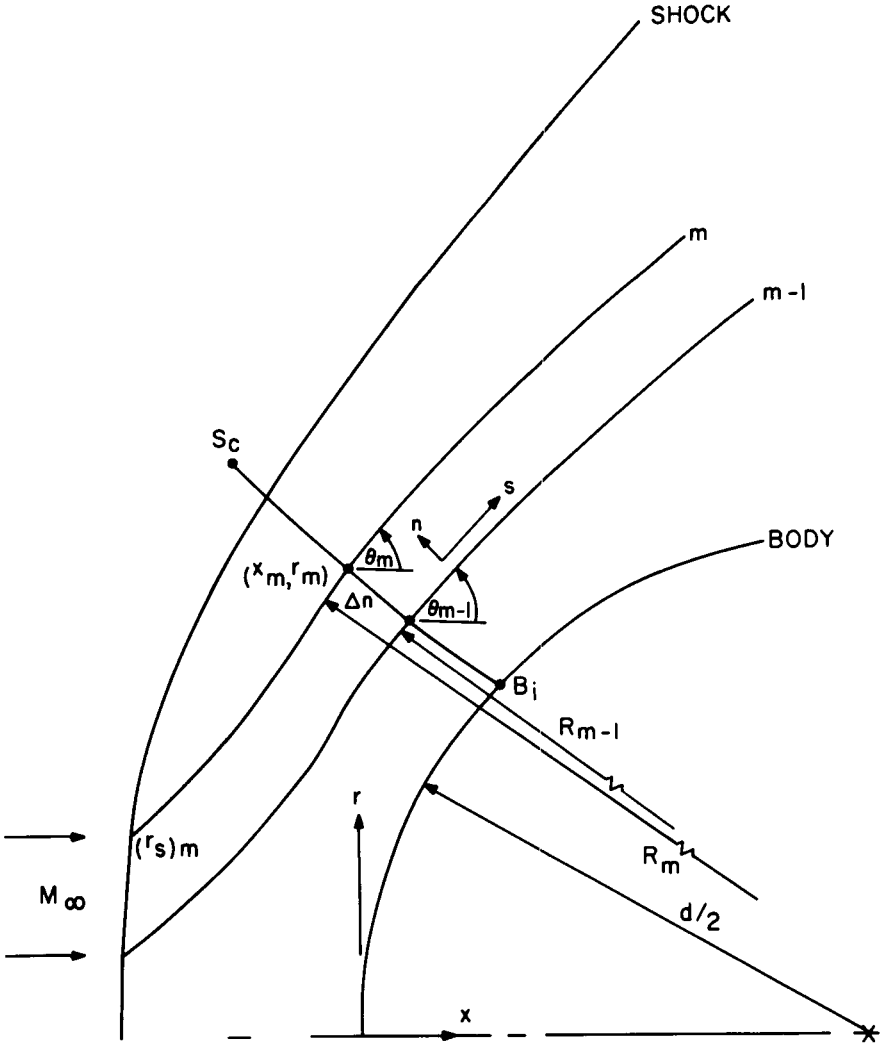


Figure 4. Notation for Transonic Calculations

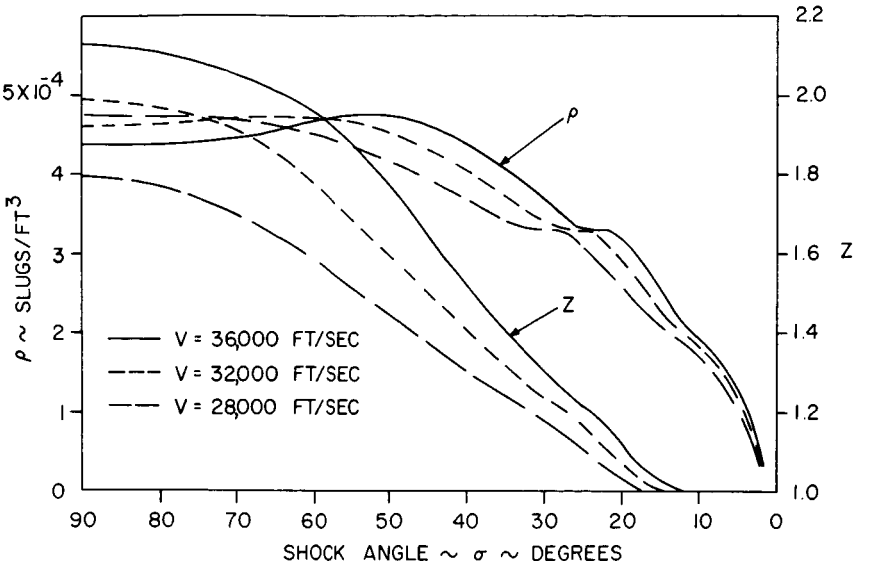


Figure 5. Density and Compressibility Behind Oblique Shock Waves

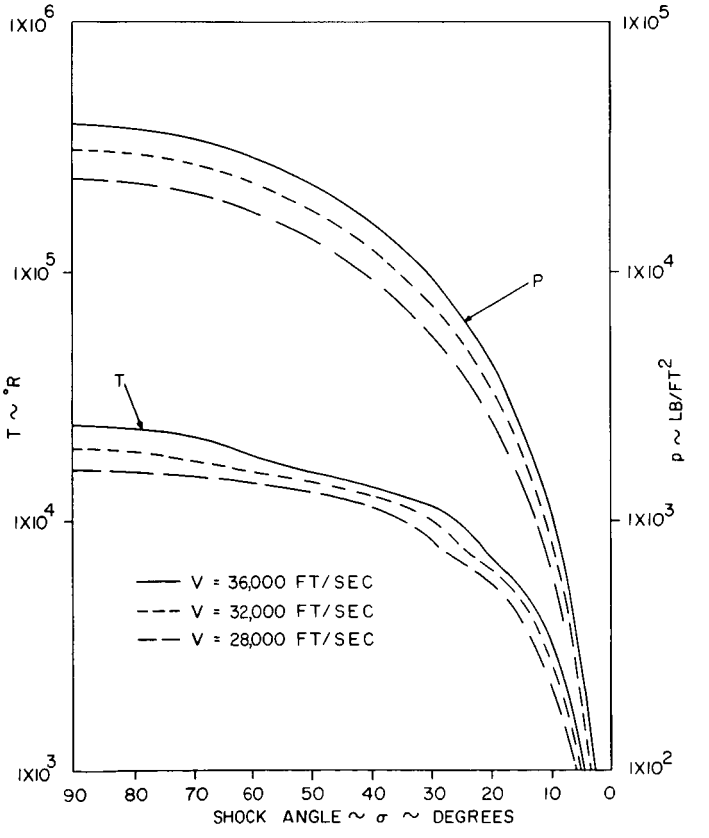


Figure 6. Temperature and Pressure Behind Oblique Shock Waves

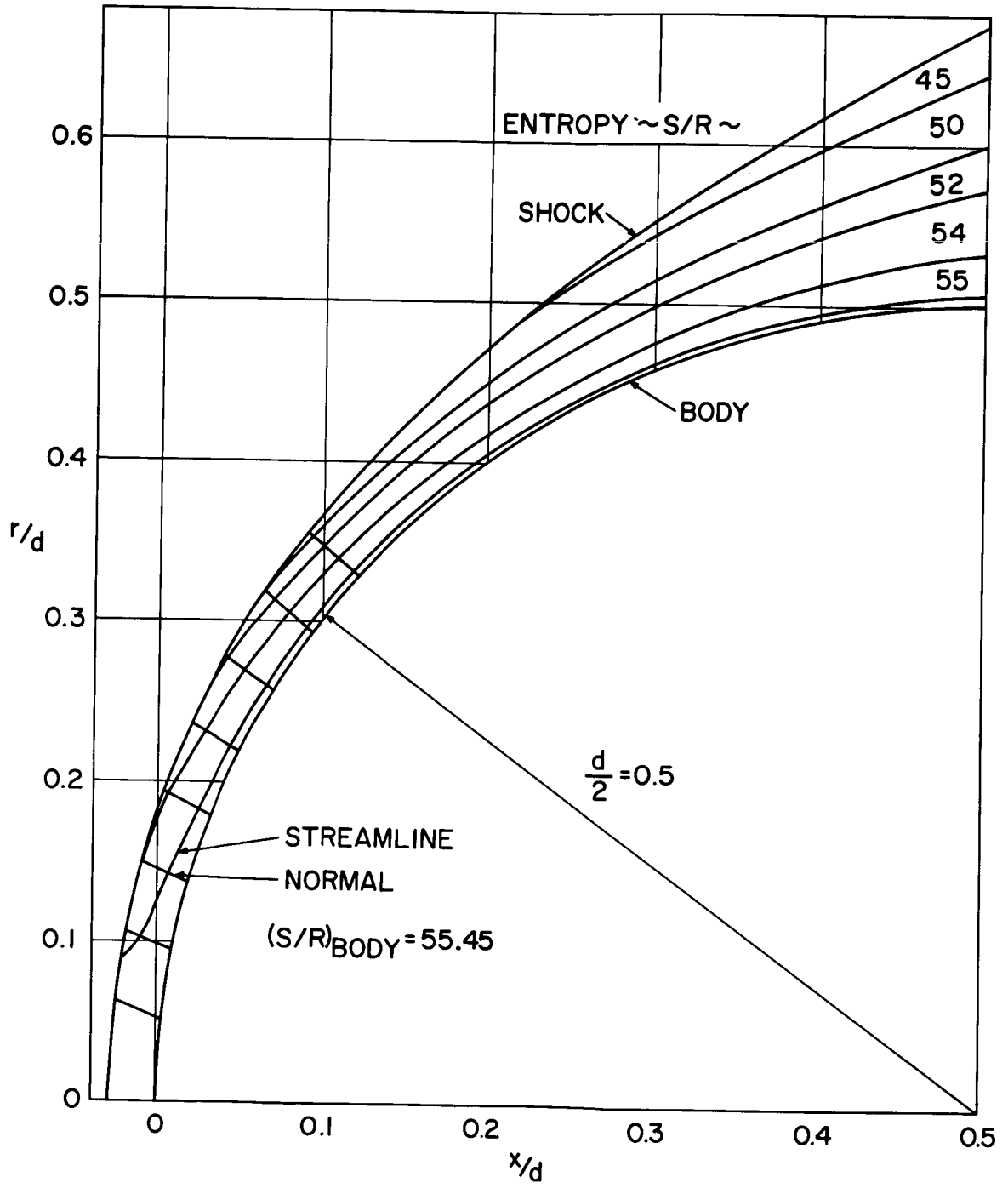


Figure 7. Transonic Normal-Streamline Grid and Streamlines in Supersonic Region of Nose

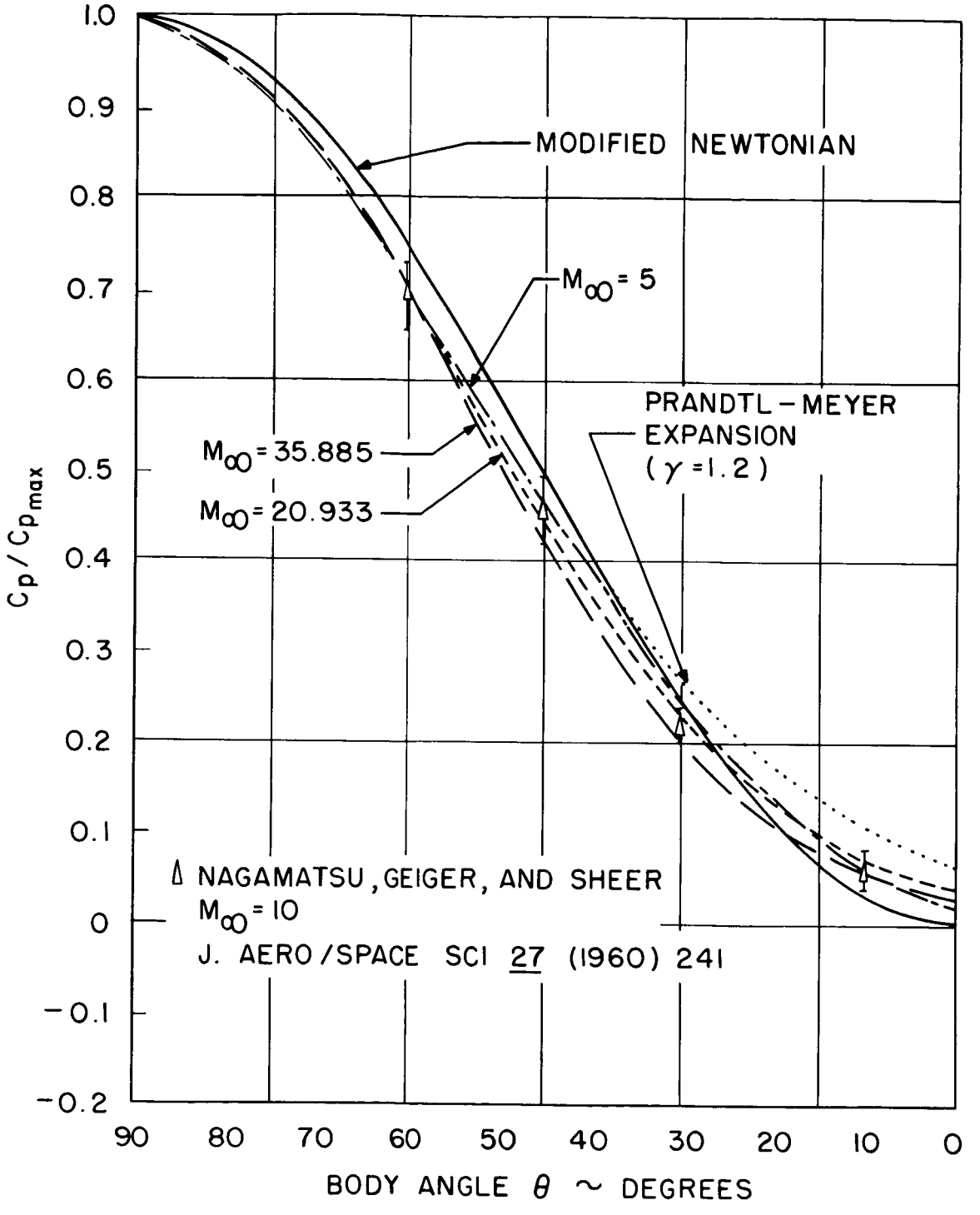


Figure 8. Pressure Distributions on Spheres: Real Gas Flow Fields and Experiment

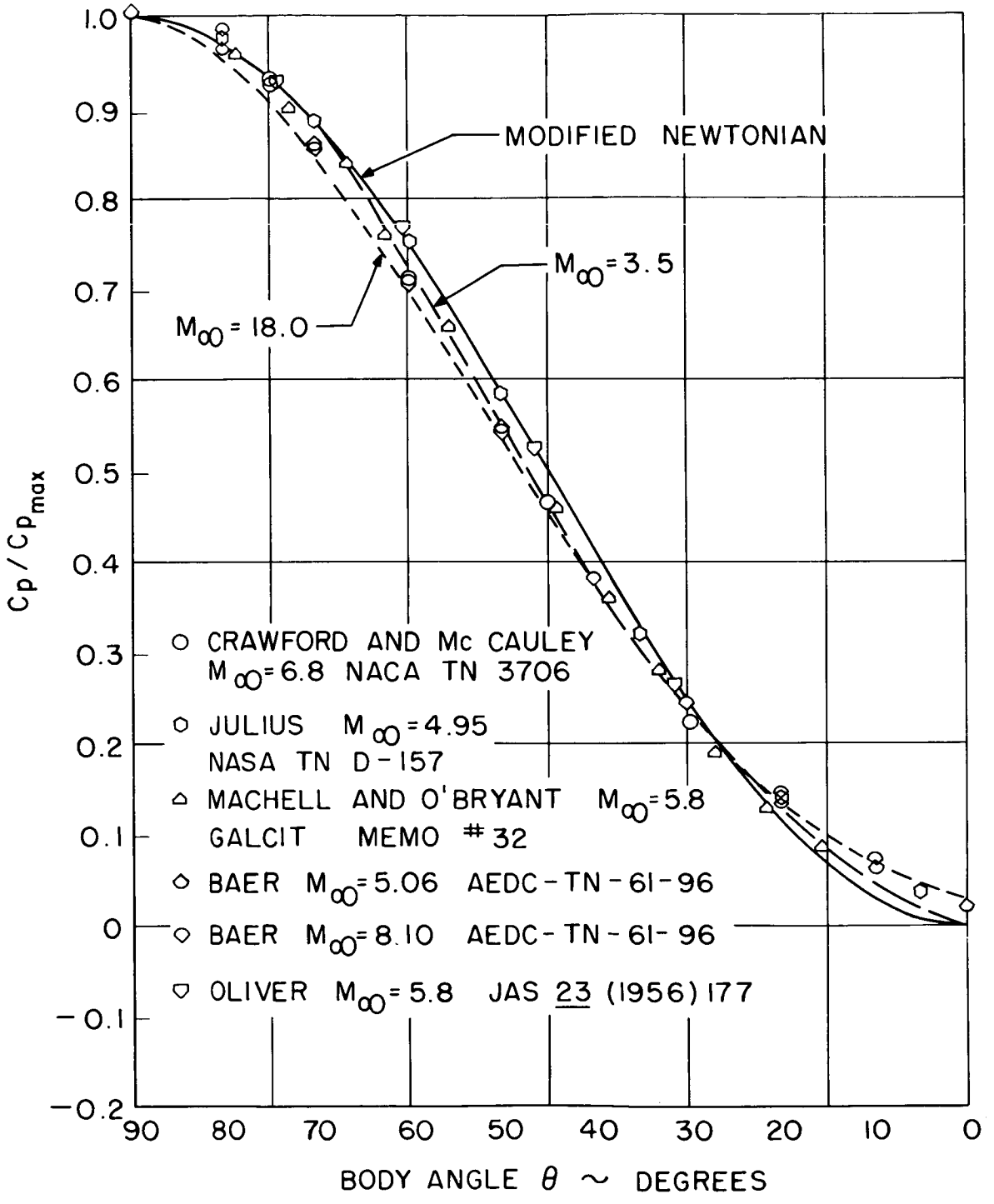


Figure 9. Pressure Distributions on Spheres: Ideal Gas Flow Fields and Experiments

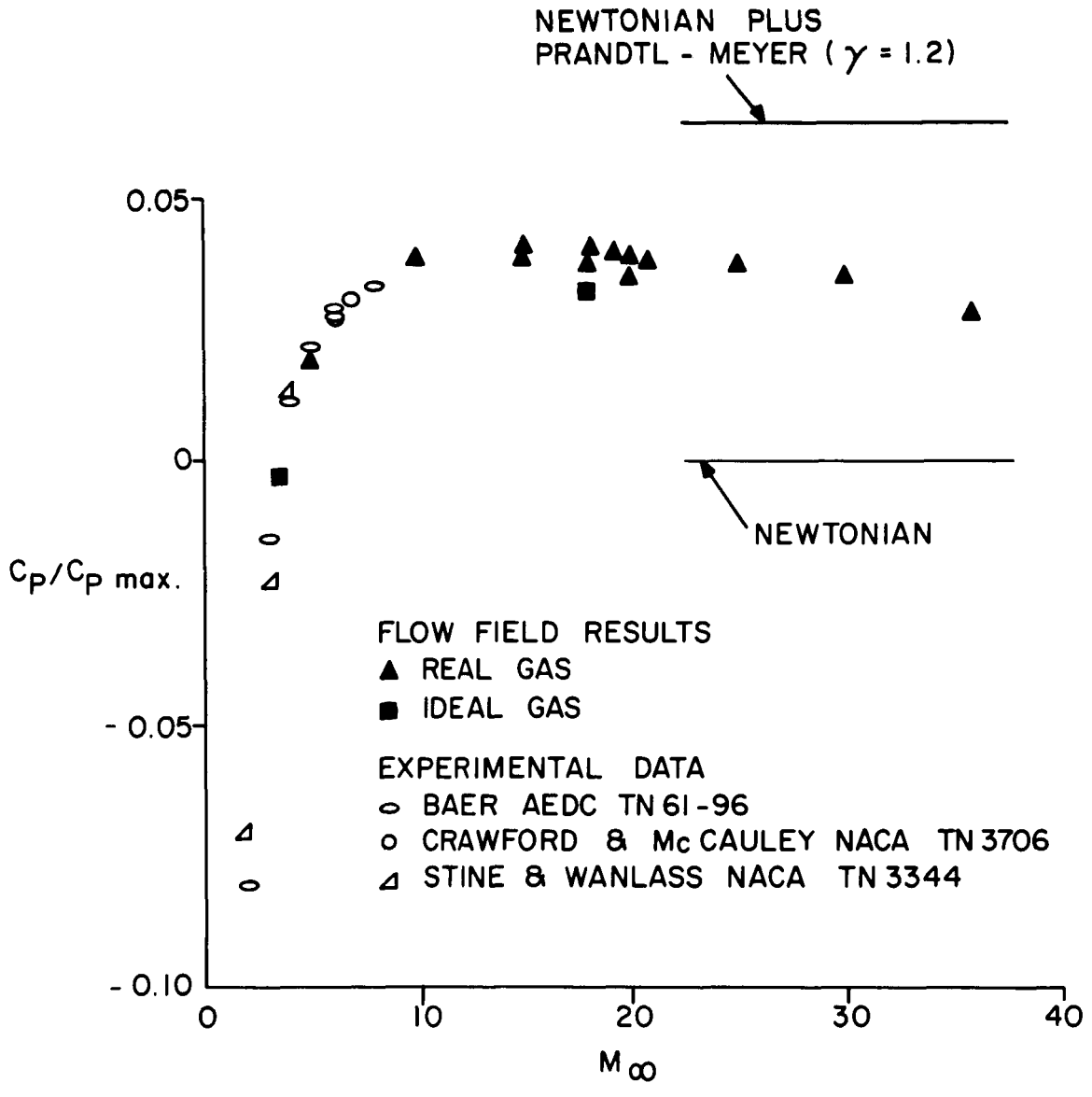


Figure 10. Shoulder Pressure Coefficients on Hemisphere-Cylinders

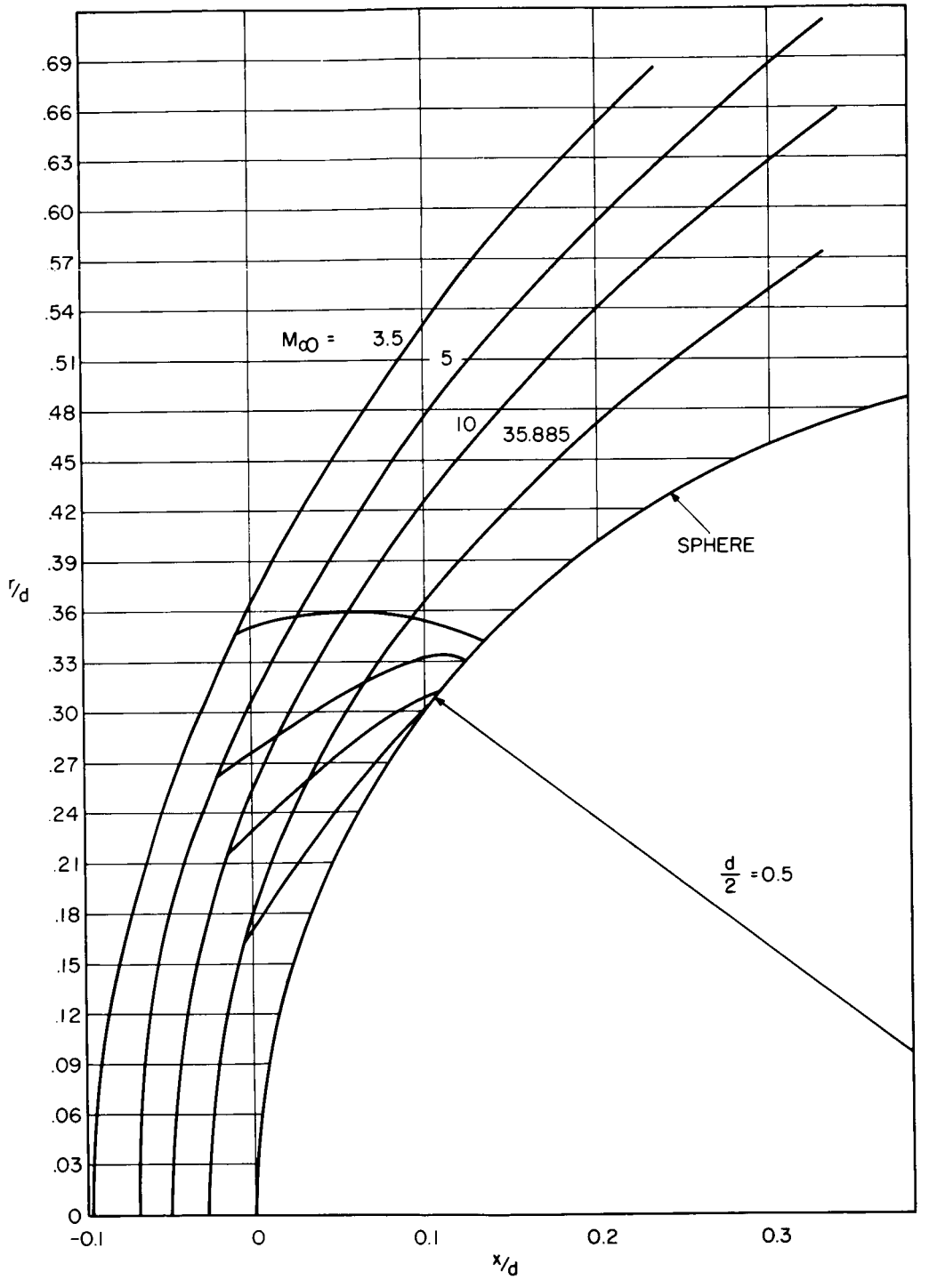


Figure 11. Shock Shapes and Sonic Lines for Four Flow Fields

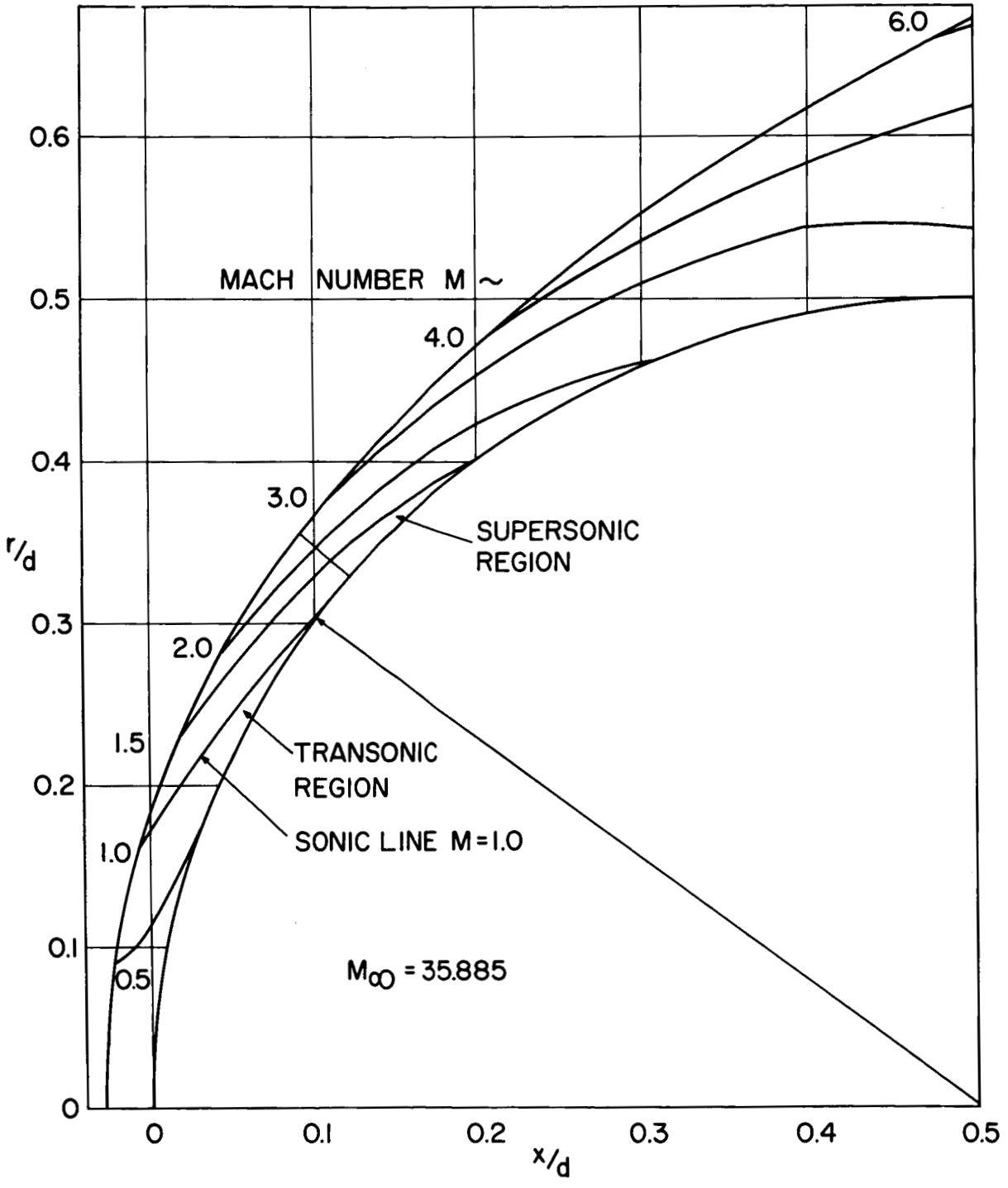


Figure 12a. Lines of Constant Mach Number for Sphere

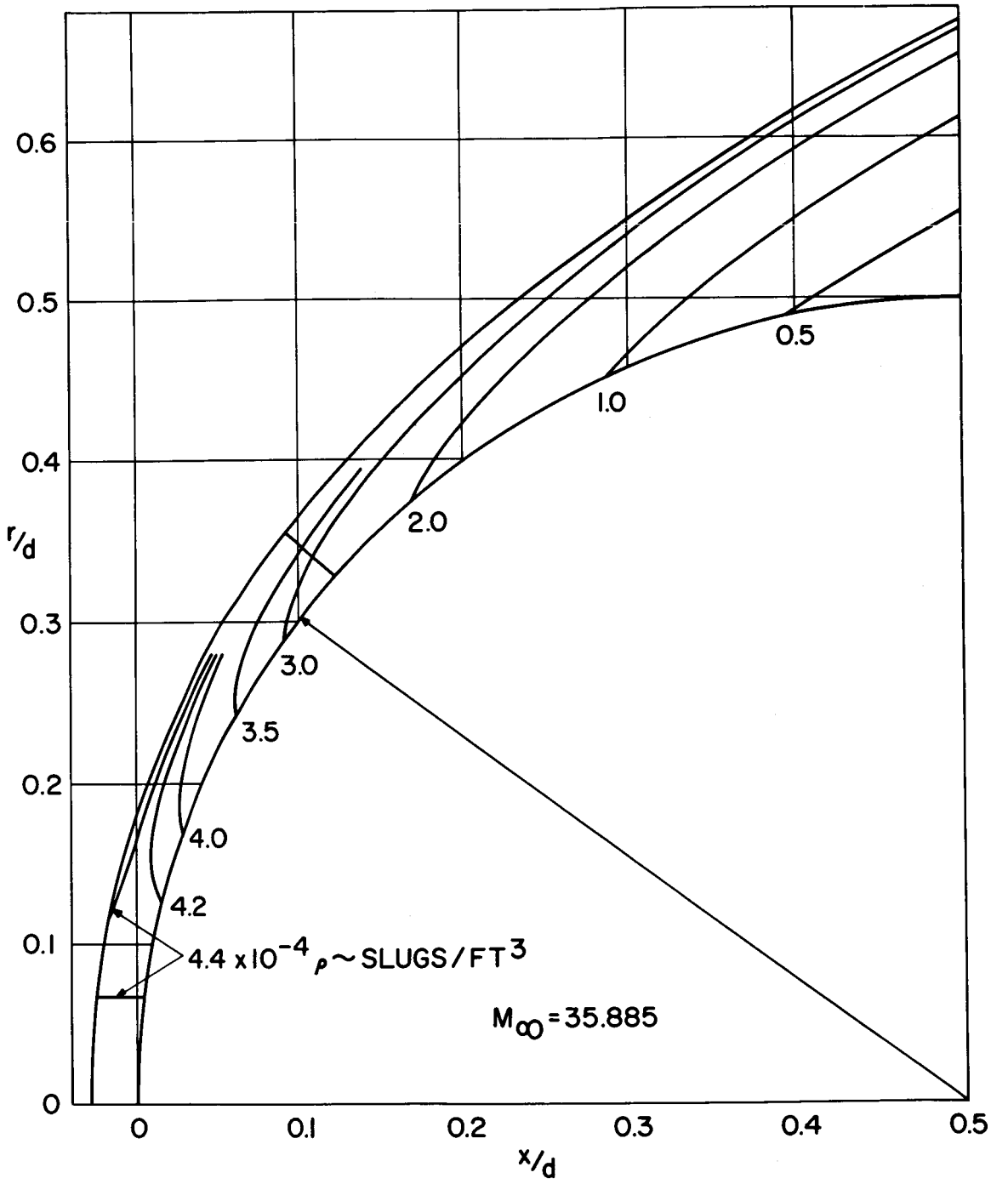


Figure 12b. Lines of Constant Density for Sphere

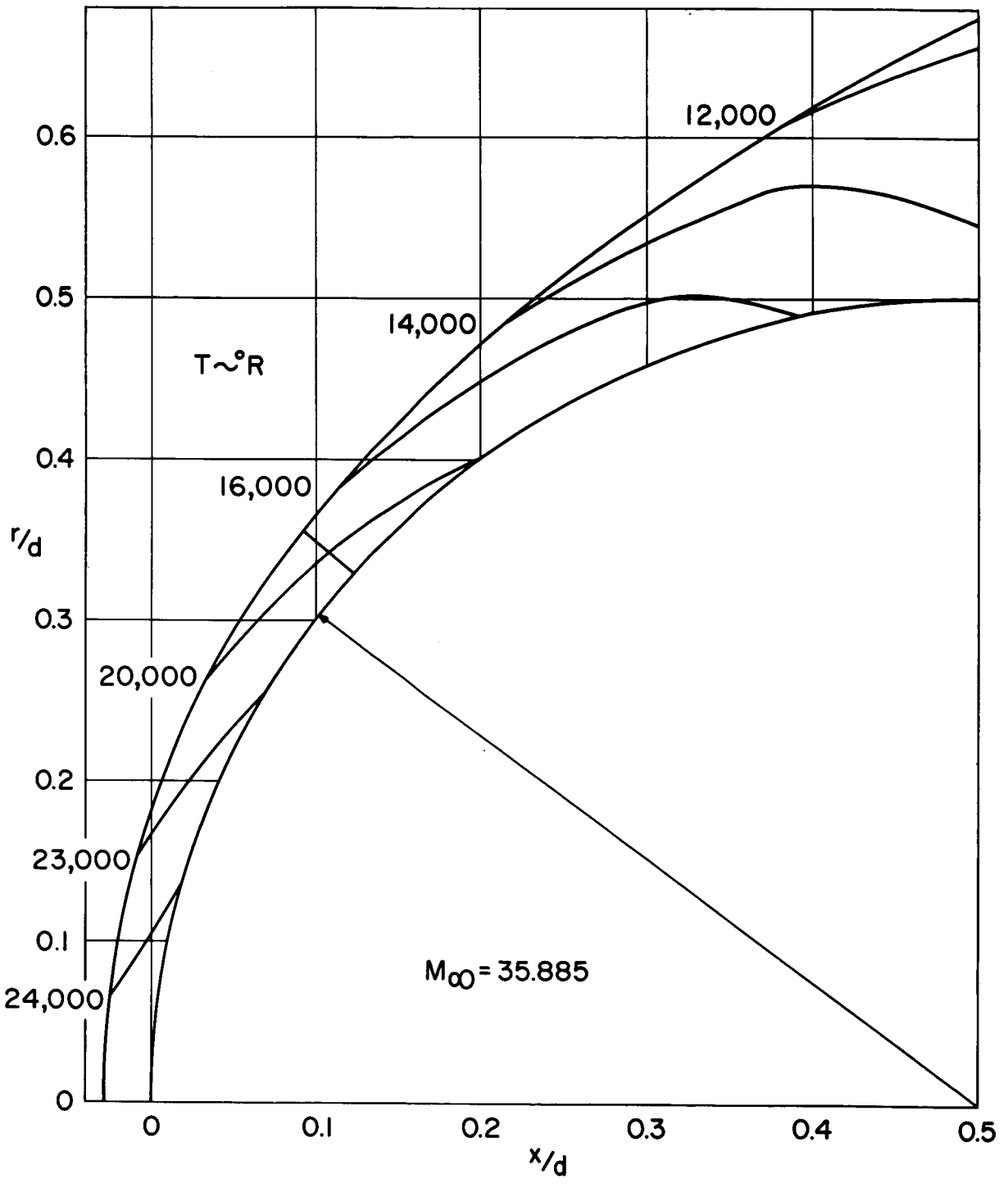


Figure 12c. Lines of Constant Temperature for Sphere

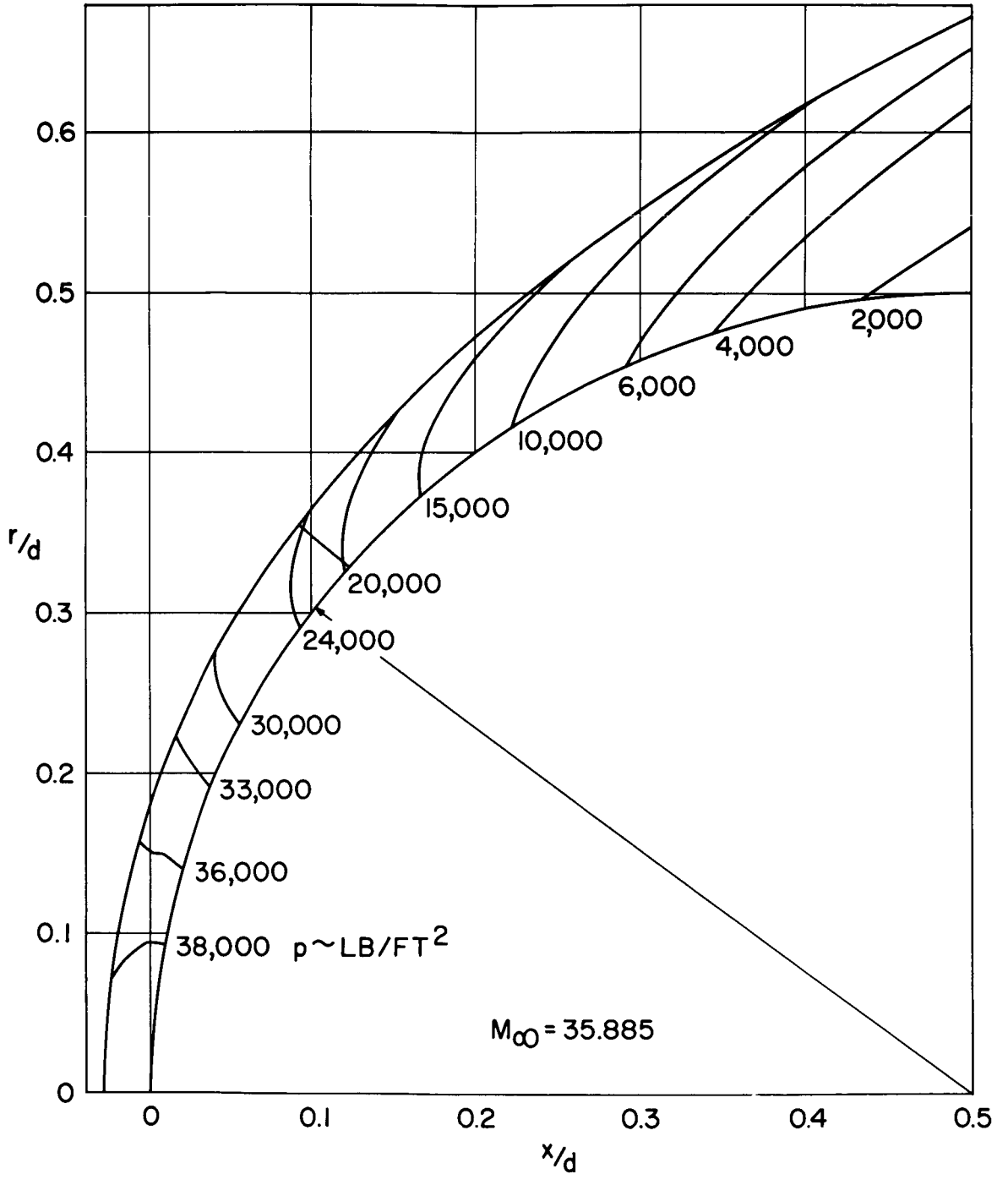


Figure 12d. Lines of Constant Pressure for Sphere

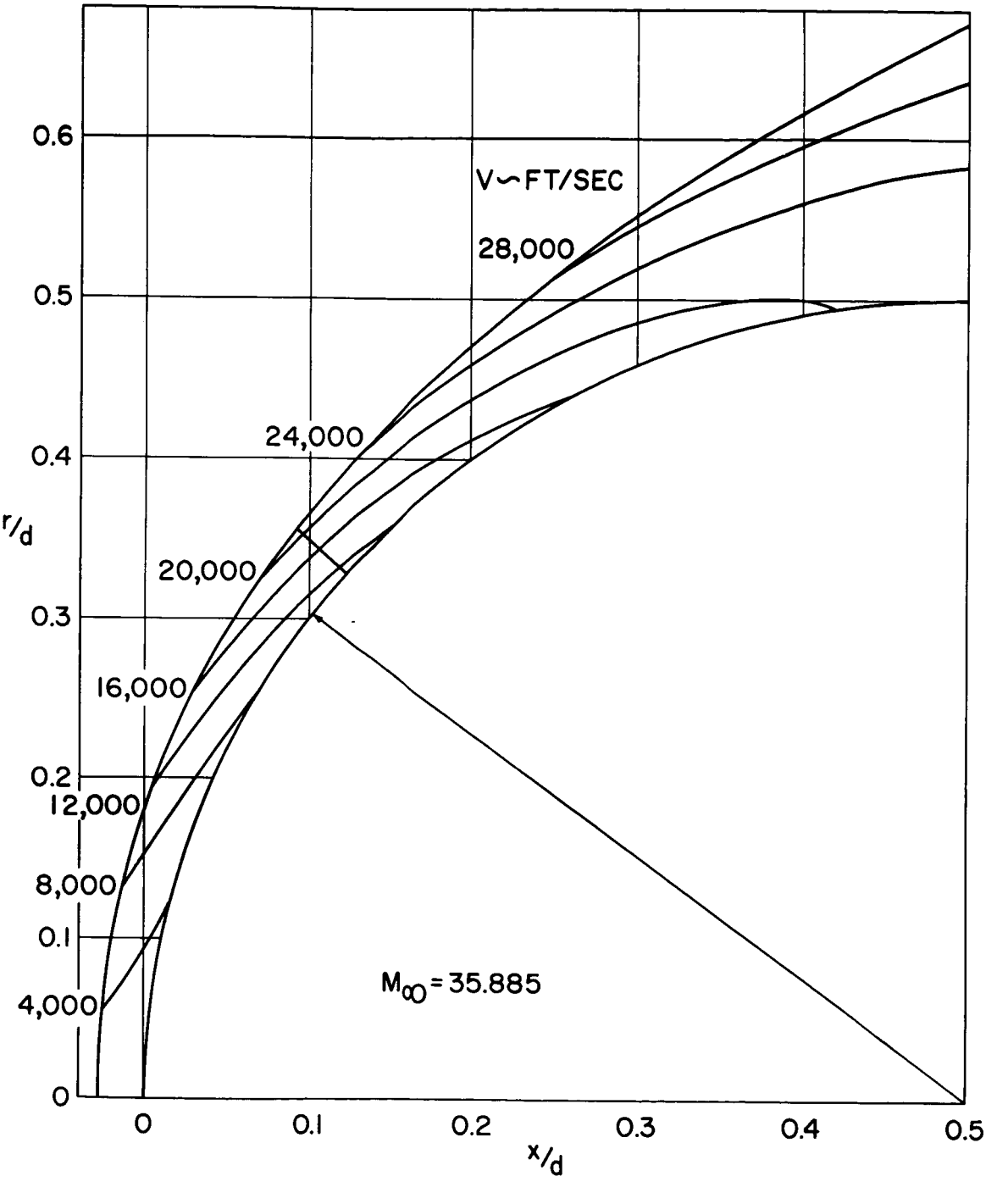


Figure 12e. Lines of Constant Velocity for Sphere

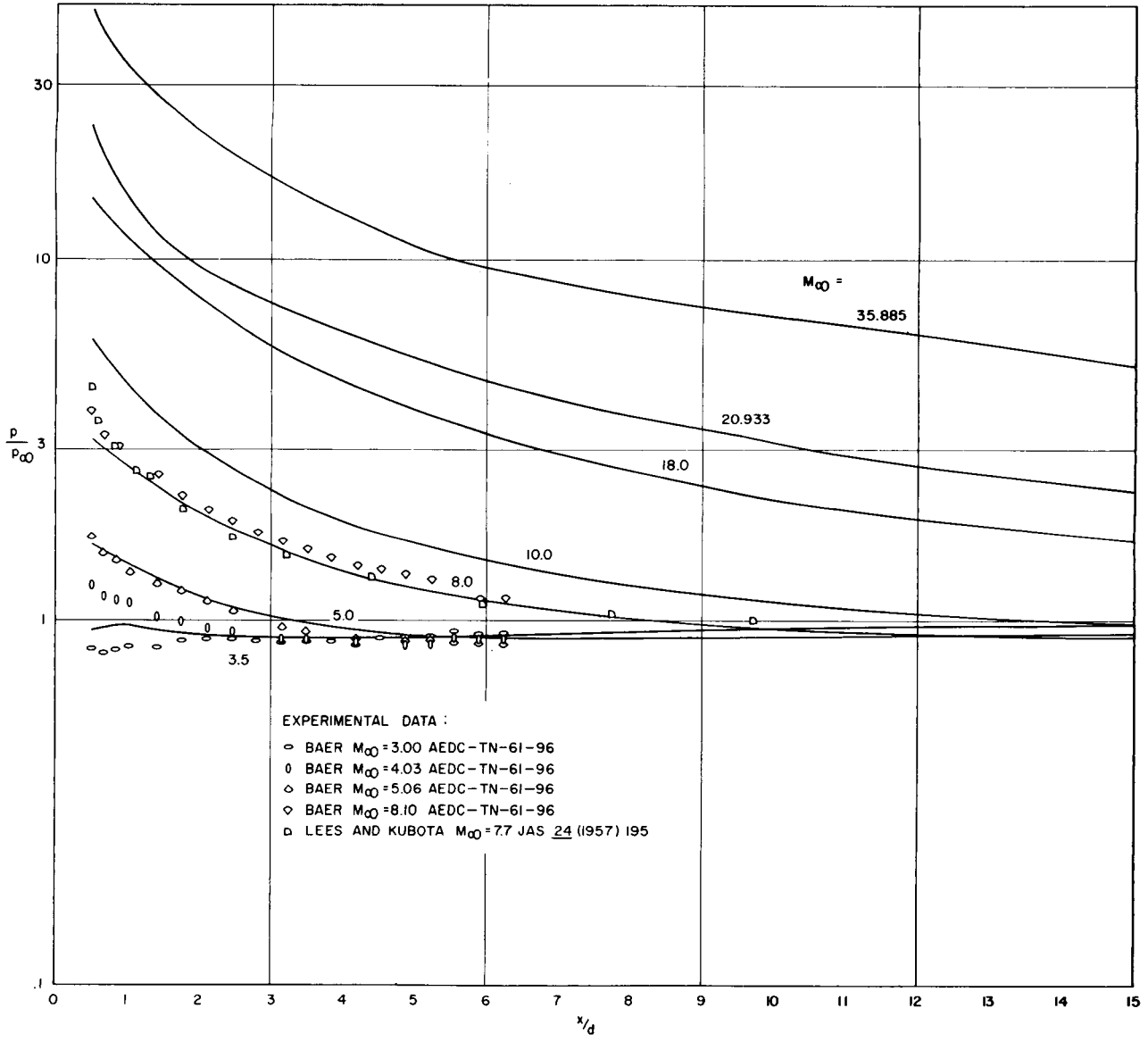


Figure 13. Pressures on Hemisphere-Cylinders: Flow Field Results and Experimental Data

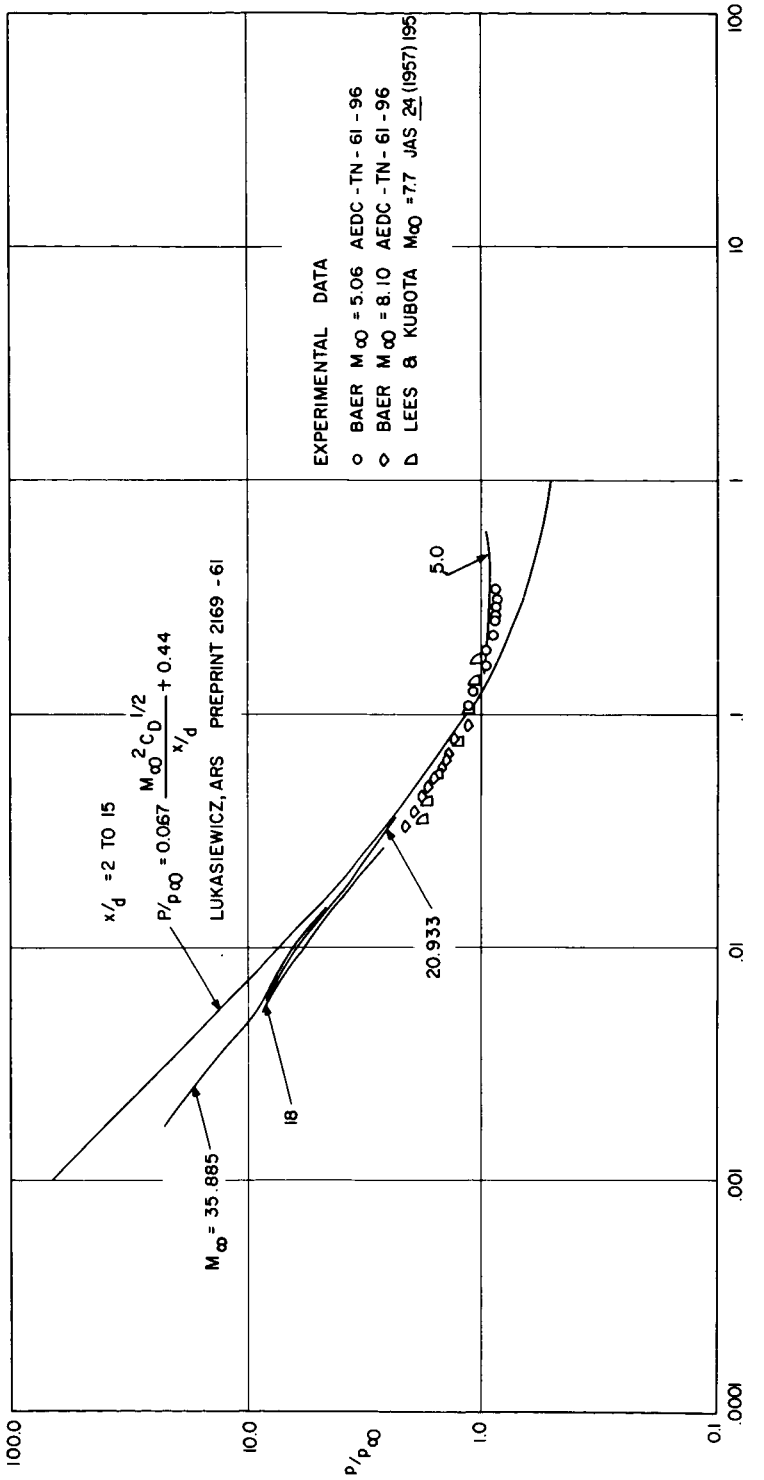


Figure 14. Body Pressure Correlation Based on Blast-Wave Parameter

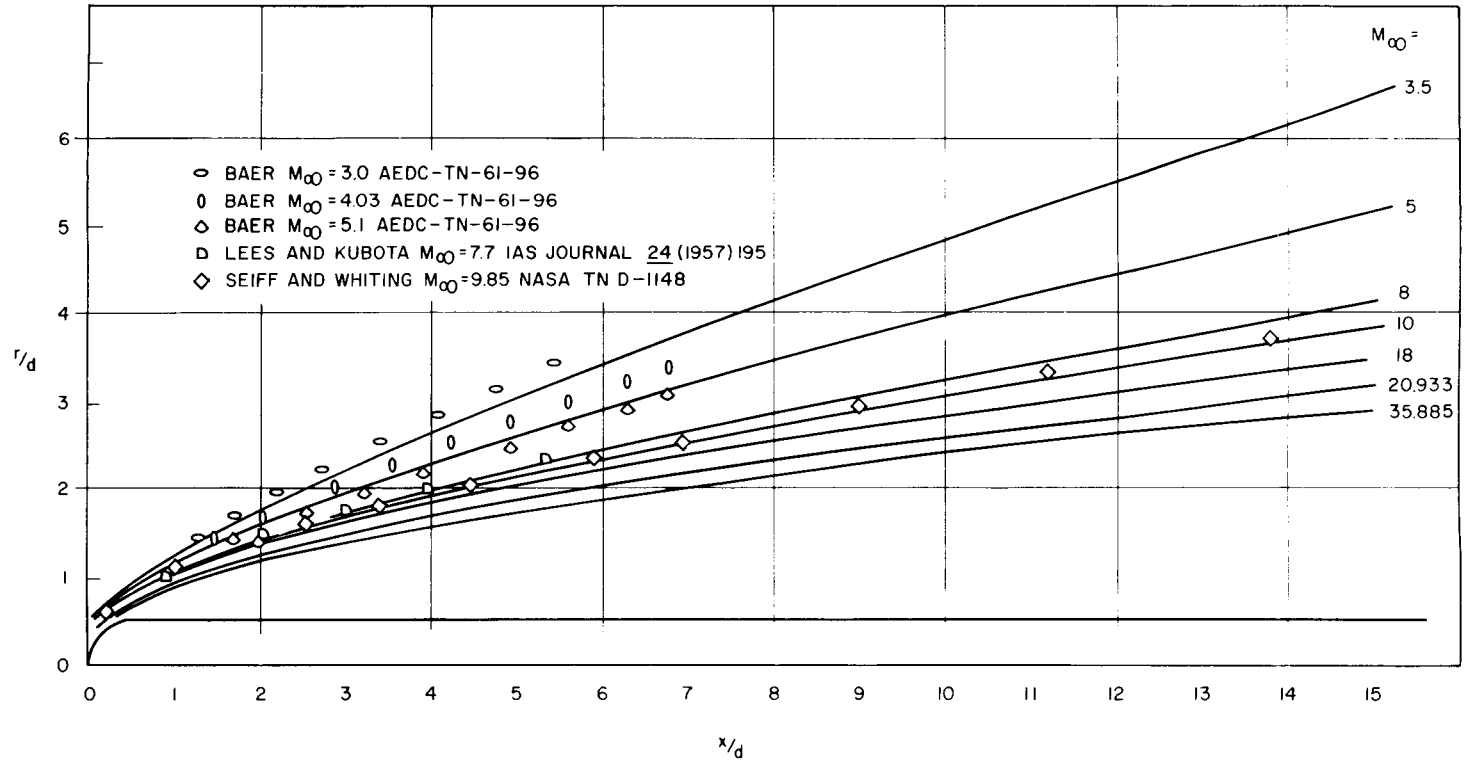


Figure 15. Shock Shapes for Hemisphere-Cylinders: Flow Field Results and Experimental Data

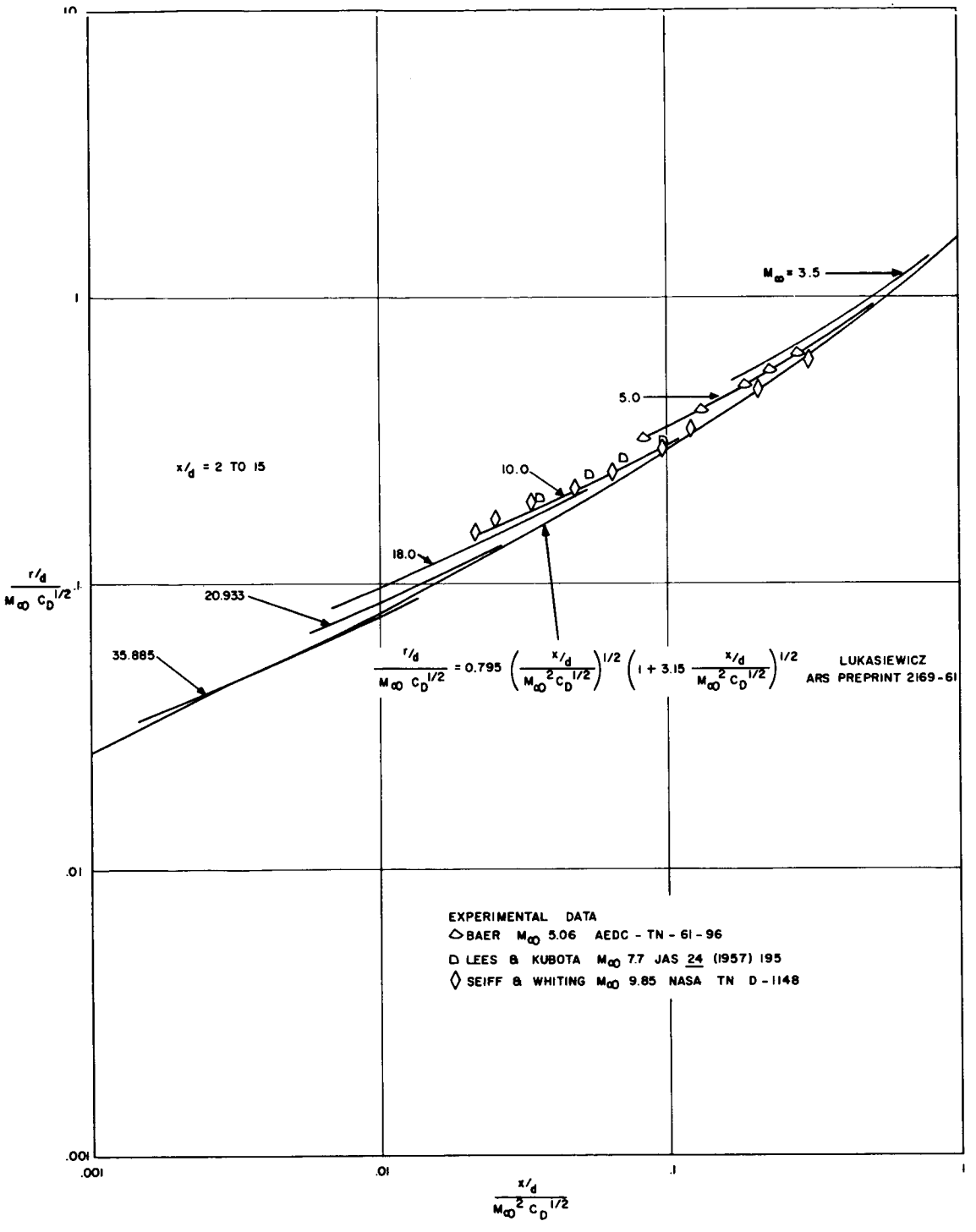


Figure 16. Shock Shape Correlation Based on Blast-Wave Parameter

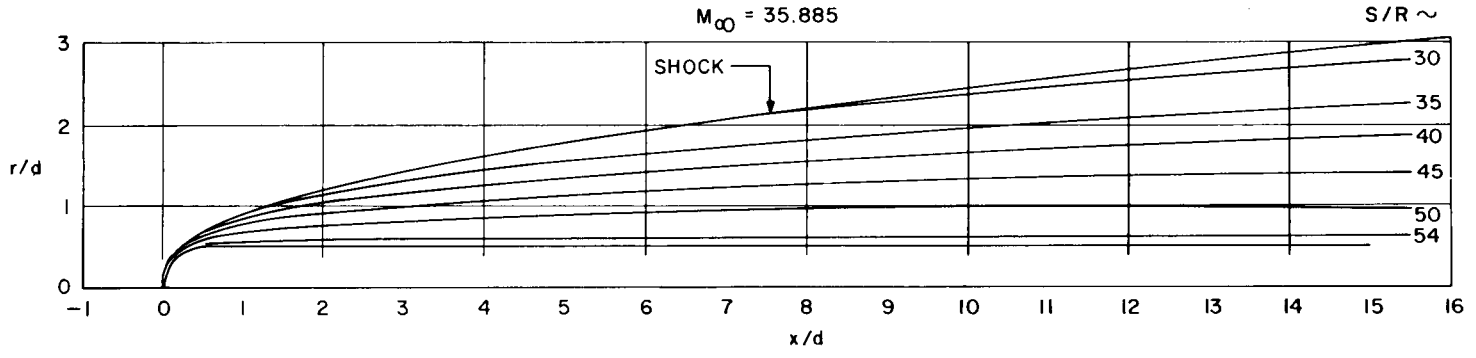


Figure 17a. Lines of Constant Entropy (Streamlines) for Cylinder

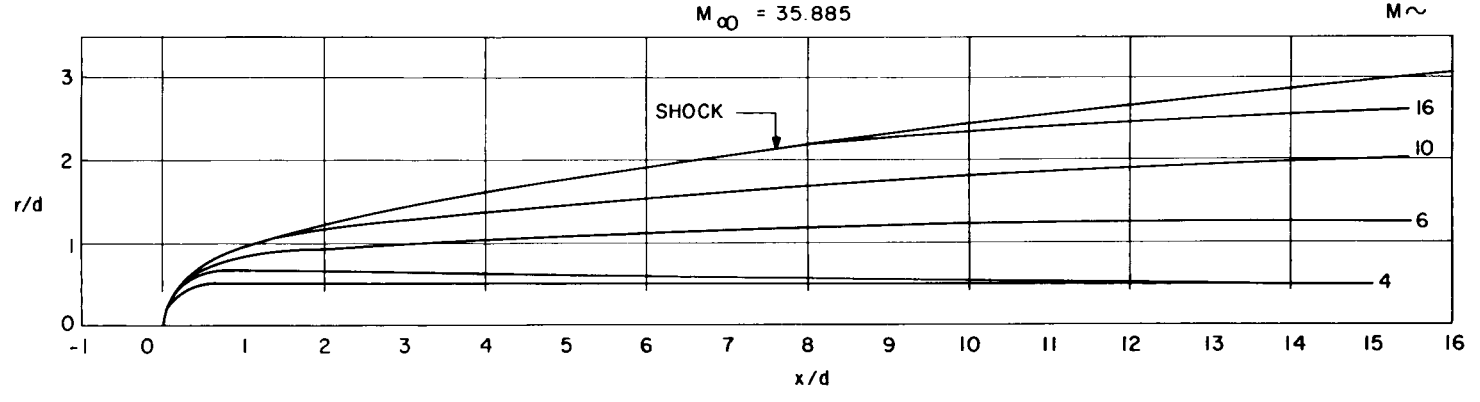


Figure 17b. Lines of Constant Mach Number for Cylinder

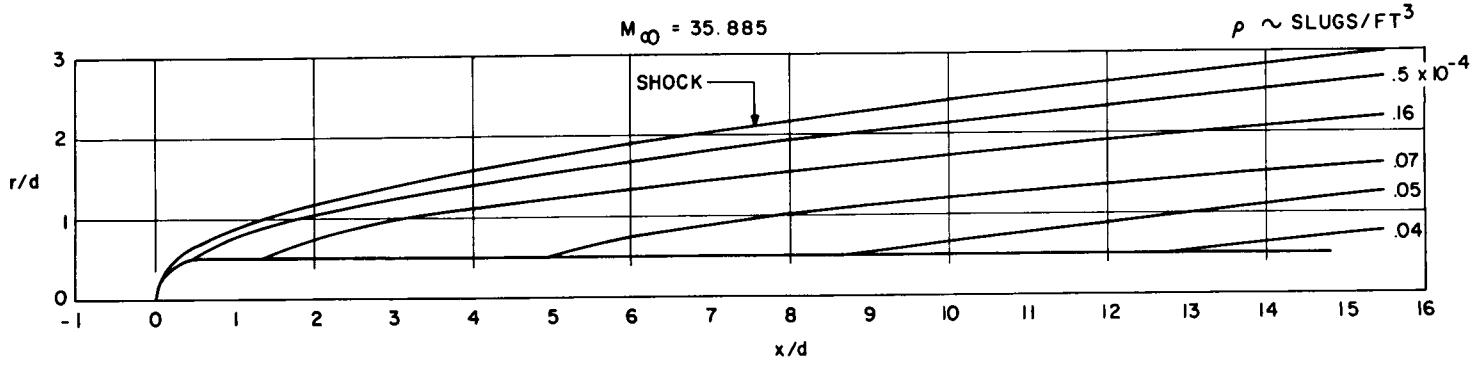


Figure 17c. Lines of Constant Density for Cylinder

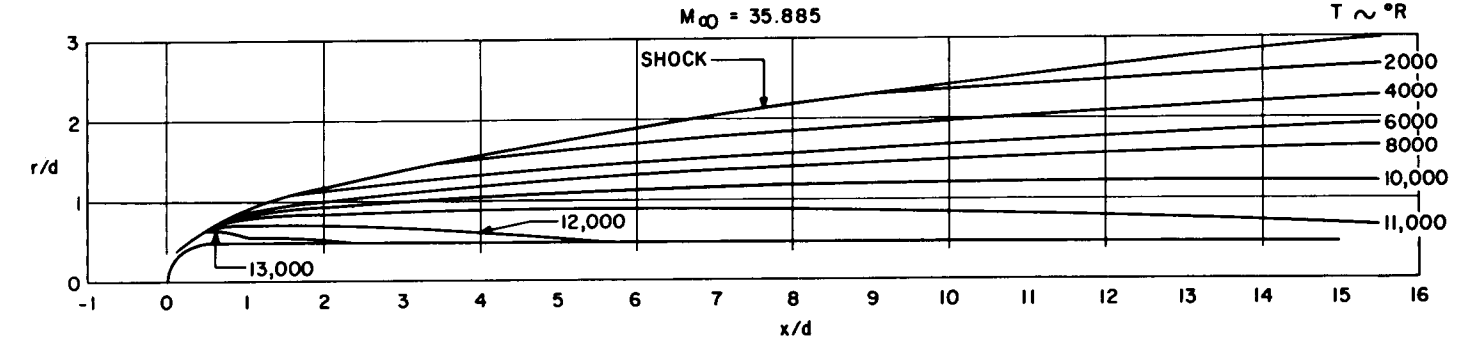


Figure 17d. Lines of Constant Temperature for Cylinder

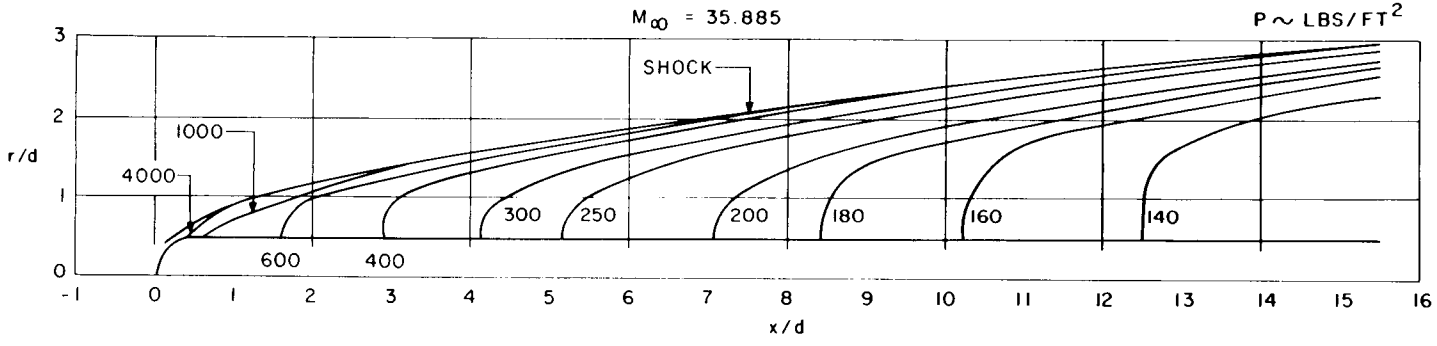


Figure 17e. Lines of Constant Pressure for Cylinder

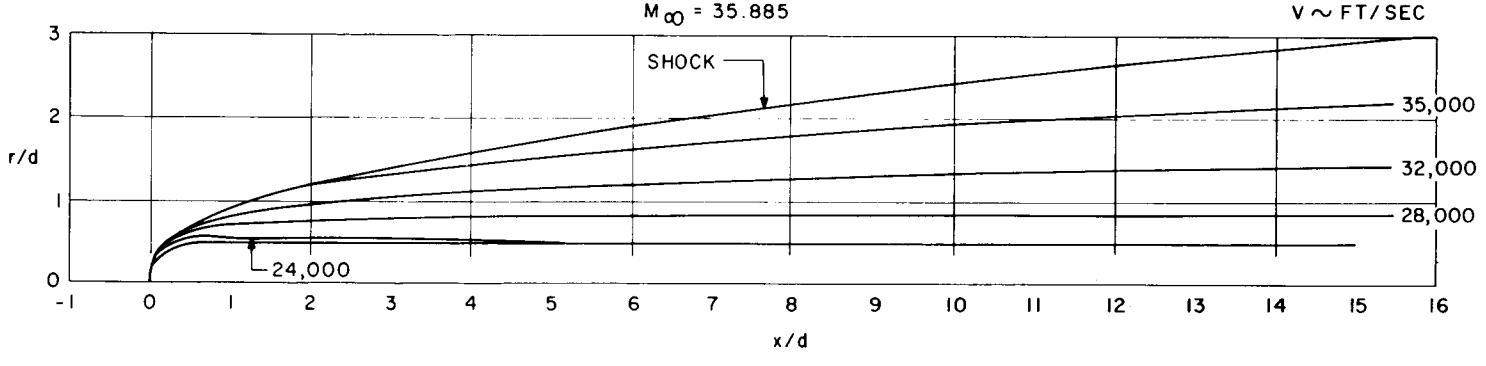


Figure 17f. Lines of Constant Velocity for Cylinder

12th STREET

J. Abel - 420
C. Anderson - 700
J. B. Arnaiz - 506
R. J. Berman - 540
J. L. Briggs - 560
E. A. Brong - 579
M. Brunner - 741
J. Cassanto - 514
P. Cilmi - 741
D. Clunies - 514
F. Costello - 421
R. S. Davis - 554
D. DeBorde - 420
J. Dunn - 411
R. Edsall - 530 (25 copies)
F. Gravalos - 8
S. F. Hill - 530
S. Kahn - 510
G. D. Katz - 528
A. A. Kirsch - 500
L. Landphair - 500
W. T. Langan - 530
R. E. Lasher - 514
D. C. Leigh - 544
W. D. McCauley - 500
L. A. Marshall - 566
W. Mertz - 420
D. Nestler - 741
E. J. Nolan - 416
M. E. O'Brien - 530
G. Rawling - 561
H. W. Ridyard - 548
H. Rie - 550
M. L. Roberts - 540
T. Shaw - 430
D. Stephenson - 551
J. D. Stewart - 709
E. M. Storer - 540
C. J. Studerus - 550
A. J. Yungman - 528
J. Zon - 561

CHESTNUT STREET

J. J. Bonasia - 5112B
W. Oberjohn - 5112B
G. Walker - 225

VALLEY FORGE

G. Arthur - 3230M
C. Baulknight - 9543L
M. Bortner - 9543L
F. Bosworth - 4605U
W. Browne - 3217M
J. Enoch - 7023A, M
P. J. Friel - 3217M
R. Geiger - 1332M
L. Gilbert - 7023A
S. Goldstein - 7222U
C. Harris - 1334M
W. G. King - 3217M
V. Langelo - 9545L
M. Lenard - 9545L
H. Lew - 9551L
E. Linkiewicz - 4605U
M. Long - 9549L
C. Mannal - 9533
M. Martin - 4620U
D. Sampson - 7023A
S. Scala - 7023A
G. Sutton - 9161
P. Thome - 7211M
H. Wachman - 1316M
K. Wan - 9537L
W. Warren - 1338
W. Wynn - 3125M
Library - 1342L (10 copies + tissue)

CABOT, CABOT, & FORBES #6

R. F. Peck - 6246
A. M. Smith - 6243
B. Wilcox - 6246

SCHENECTADY

I. H. Edelfelt - Rm. 621 Bldg. 37
General Engineering Lab., Schenectady, N.Y.
D. W. Jones - Rm. 621 Bldg. 37
General Engineering Lab., Schenectady, N.Y.
TIS Center 2 copies + 6 title pages - Schenectady